Check for updates

53BP1–shieldin-dependent DSB processing in BRCA1-deficient cells requires CST–Polα–primase fill-in synthesis

Zachary Mirman [1], Nanda Kumar Sasi[1], Ashleigh King[2], J. Ross Chapman [2] and Titia de Lange [1✉]

The efficacy of poly(ADP)-ribose polymerase 1 inhibition (PARPi) in BRCA1-deficient cells depends on 53BP1 and shieldin, which have been proposed to limit single-stranded DNA at double-strand breaks (DSBs) by blocking resection and/or through CST–Polα–primase-mediated fill-in. We show that primase (like 53BP1–shieldin and CST–Polα) promotes radial chromosome formation in PARPi-treated BRCA1-deficient cells and demonstrate shieldin–CST–Polα–primase-dependent incorporation of BrdU at DSBs. In the absence of 53BP1 or shieldin, radial formation in BRCA1-deficient cells was restored by the tethering of CST near DSBs, arguing that in this context, shieldin acts primarily by recruiting CST. Furthermore, a SHLD1 mutant defective in CST binding (SHLD1Δ) was non-functional in BRCA1-deficient cells and its function was restored after reconnecting SHLD1Δ to CST. Interestingly, at dysfunctional telomeres and at DNA breaks in class switch recombination where CST has been implicated, SHLD1Δ was fully functional, perhaps because these DNA ends carry CST recognition sites that afford SHLD1-independent binding of CST. These data establish that in BRCA1-deficient cells, CST–Polα–primase is the major effector of shieldin-dependent DSB processing.

BRCA1 and 53BP1 are multifaceted DNA-damage response proteins that participate in the repair of double-strand breaks (DSBs), in part by affecting the length of 3′ single-stranded (ss) DNA overhangs[1]. In classical non-homologous end-joining, minimally processed ends are ligated by ligase 4 (encoded by *Lig4*), a rapid and largely accurate process that is active throughout the cell cycle[2]. Homology-directed repair (HDR), in contrast, requires a 3′ ss overhang and its coating by RAD51 for strand invasion of a homologous template[3,4]. BRCA1-deficient cells show minimal RAD51 loading at DSBs and are sensitive to PARPi[5–7]. In the absence of BRCA1-mediated HDR, some PARPi-induced DSBs are mis-rejoined into characteristic 'radial' chromosomes through the action of 53BP1[8,9].

53BP1 has been proposed to control DSB repair pathway choice and/or the fidelity of DSB repair[1,10]. The role of 53BP1 in limiting the formation of 3′ overhangs depends on RIF1 and the shieldin complex (comprising REV7, SHLD1, SHLD2 and SHLD3)[11–22]. Similar to the effects of the loss of 53BP1 or RIF1, disruption of shieldin components reverses the hallmarks of PARPi in BRCA1-deficient cells. Purified SHLD2–SHLD1 complexes can bind ssDNA of 60–100 nucleotides[21–24], an activity that has been proposed to underlie the ability of the 53BP1 pathway to limit the formation of ssDNA overhangs by blocking nucleases that attack the 5′ end[10,22]. Nevertheless, direct evidence that shieldin blocks 5′ end resection is lacking.

In a second model, shieldin limits ssDNA at DSBs by recruiting CST–Polα–primase to counteract resection via fill-in synthesis. Supporting this model, shieldin directly interacts with CST (comprising CTC1, STN1 and TEN1), which is a Polα-associated complex. Furthermore, depletion of CST or pharmacological inhibition of Polα reduces the formation of radial chromosomes in BRCA1-deficient cells treated with PARPi[19].

We set out to distinguish between these two models in BRCA1-deficient cells. We demonstrate a role for primase in

promoting PARPi-induced radial chromosomes via degradation of PRIM1 induced by auxin (3-indole-acetic acid (IAA)). Consistent with fill-in synthesis, incorporation of bromodeoxyuridine (BrdU) occurred at FOKI-induced DSBs, and a proximity ligation assay (PLA) for BrdU and γH2AX enabled direct visualization of shieldin-mediated and Polα–primase-mediated fill-in synthesis at chromosome breaks in BRCA1-deficient cells. Artificially targeting the STN1 subunit of CST to DSBs induced radial chromosome formation in PARPi-treated BRCA1-deficient cells despite the absence of 53BP1 and shieldin. To further test the involvement of CST downstream of shieldin, we generated a separation of function mutation in SHLD1 that disrupts its interaction with CTC1 and its ability to recruit CST to DSBs. This SHLD1Δ mutant completely abrogated the function of shieldin in BRCA1-deficient cells, and its function could be restored by SNAP–HALO tagging of SHLD1Δ and CTC1 and forcing their interaction by chemical-induced dimerization. Remarkably, SHLD1Δ appeared to be fully functional in processing DSBs in class switch recombination (CSR) and at dysfunctional telomeres, a result we explain based on the unique feature of these DNA ends in that they carry CST recognition sites. These results demonstrate that CST–Polα–primase fill-in synthesis is a major determinant of shieldin-dependent DSB processing in BRCA1-deficient cells.

Results

Primase affects radial formation and RAD51 loading in BRCA1-deficient cells. To determine whether primase, like CST and Polα, is involved in the processing of DSBs downstream of 53BP1–shieldin, we generated p53–Rb-deficient RPE1 cells in which the endogenous PRIM1 subunit of primase can be rapidly degraded using the TIR–auxin system[25] (Extended Data Fig. 1). After CRISPR-mediated targeting of *BRCA1*, PRIM1 was degraded in G2-arrested cells (Fig. 1a). BRCA1-deficient cells, but not

[1]Laboratory for Cell Biology and Genetics, Rockefeller University, New York, NY, USA. [2]Medical Research Council (MRC) Molecular Haematology Unit, Weatherall Institute of Molecular Medicine, University of Oxford, Oxford, UK. ✉e-mail: delange@rockefeller.edu
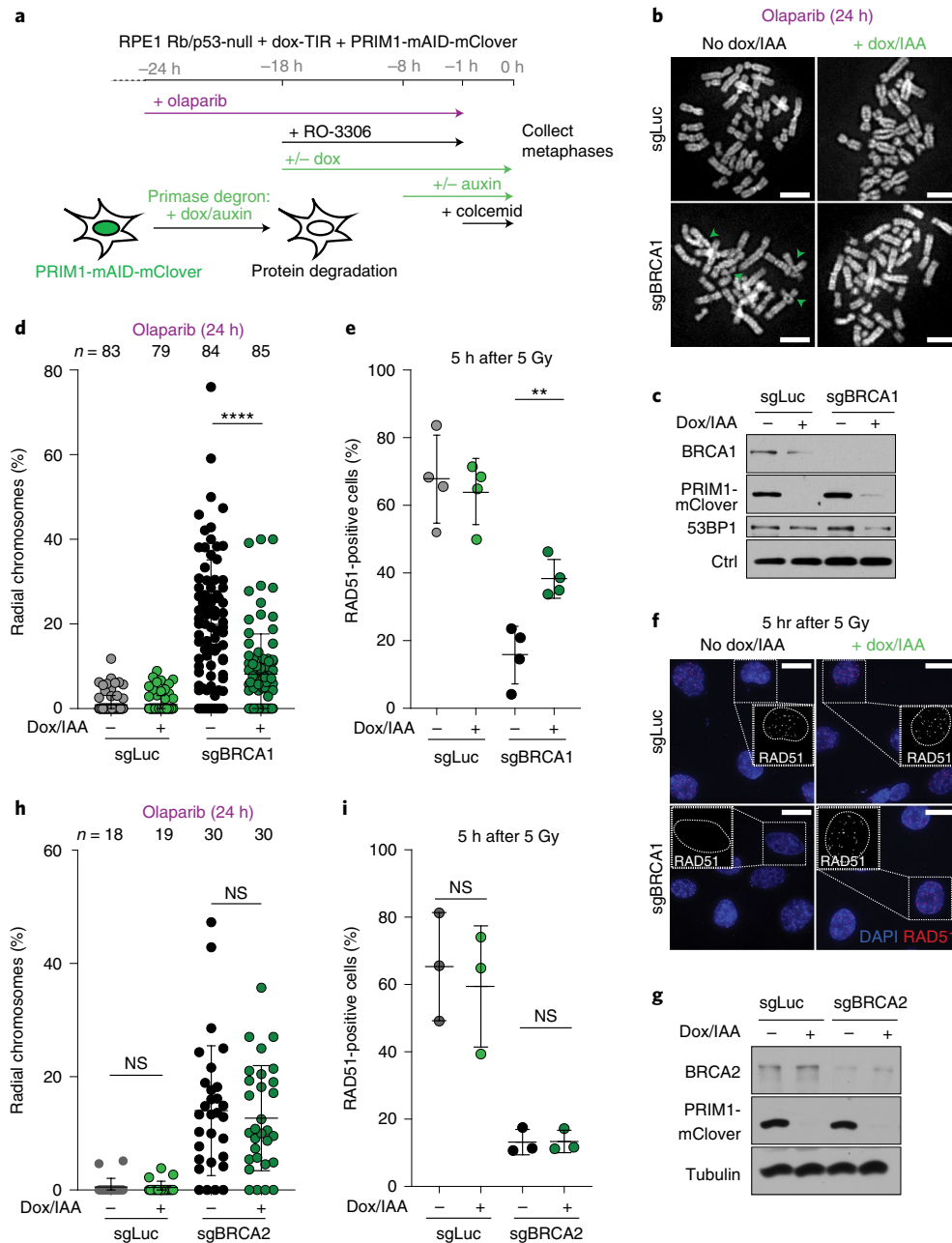
Fig. 1 | Primase promotes radials and blocks RAD51 loading in BRCA1-deficient cells. a, Schematic of the timeline of auxin-induced degradation of PRIM1 in G2-arrested RPE1 cells treated with PARPi. **b**, Representative images of DAPI-stained metaphase spreads from RPE1 PRIM1-mAID-mClover cells with the indicated treatments. Green arrowheads indicate aberrant radial chromosomes. Scale bars, 5 μm. **c**, Immunoblot for BRCA1 and GFP (mClover-PRIM1) in cells as in **a** treated with control (sgLuc) or BRCA1 (sgBRCA1) bulk CRISPR KO. Ctrl, nonspecific band from GFP blot. **d**, Quantification of the percent of chromosomes involved in radial structures. The number of metaphases analysed per condition (n) is indicated. **e**, Quantification of the percent of RAD51-positive cells (with 10 or more RAD51 foci per nucleus) 5 h after 5 Gy IR. n = four independent experiments. **f**, Representative images of IF for RAD51 in cells as in **e** with the indicated treatments. Scale bars, 20 μm. **g**, Immunoblot for BRCA2 and GFP (mClover-PRIM1) in cells as in **a** treated with control (sgLuc) or BRCA2 (sgBRCA2) bulk CRISPR KO. **h**, Quantification of the percent of chromosomes involved in radial structures (as in **d**). The number of metaphases analysed per condition (n) is indicated. **i**, Quantification of the percent of RAD51-positive cells, as in **e**, in the indicated cells. n = three independent experiments. Data shown in **b–d** and **f–i** are representative of three independent experiments. All statistical analysis based on two-tailed Welch's t-test. *P < 0.05, **P < 0.01, ***P < 0.001, ****P < 0.0001, NS, not significant. All means are indicated with centre bars and s.d. with error bars.

the luciferase CRISPR-targeted control, showed characteristic PARPi-induced radial chromosomes. PRIM1 degradation significantly diminished radial formation in the BRCA1-deficient cells (Fig. 1b–d) and restored their ability to form RAD51 foci after ionizing radiation (IR) (Fig. 1e,f and Extended Data Fig. 2a,b). As a control, we monitored the effect of PRIM1 degradation in the

setting of BRCA2 deficiency, whereby 53BP1 deletion does not reverse the effects of BRCA2 loss[8]. While PARPi treatment induced radial chromosomes in BRCA2-deficient cells, these were not diminished by the loss of PRIM1 (Fig. 1g,h). Furthermore, PRIM1 degradation did not restore RAD51 loading in BRCA2-deficient cells (Fig. 1i and Extended Data Fig. 2c). These results establish that
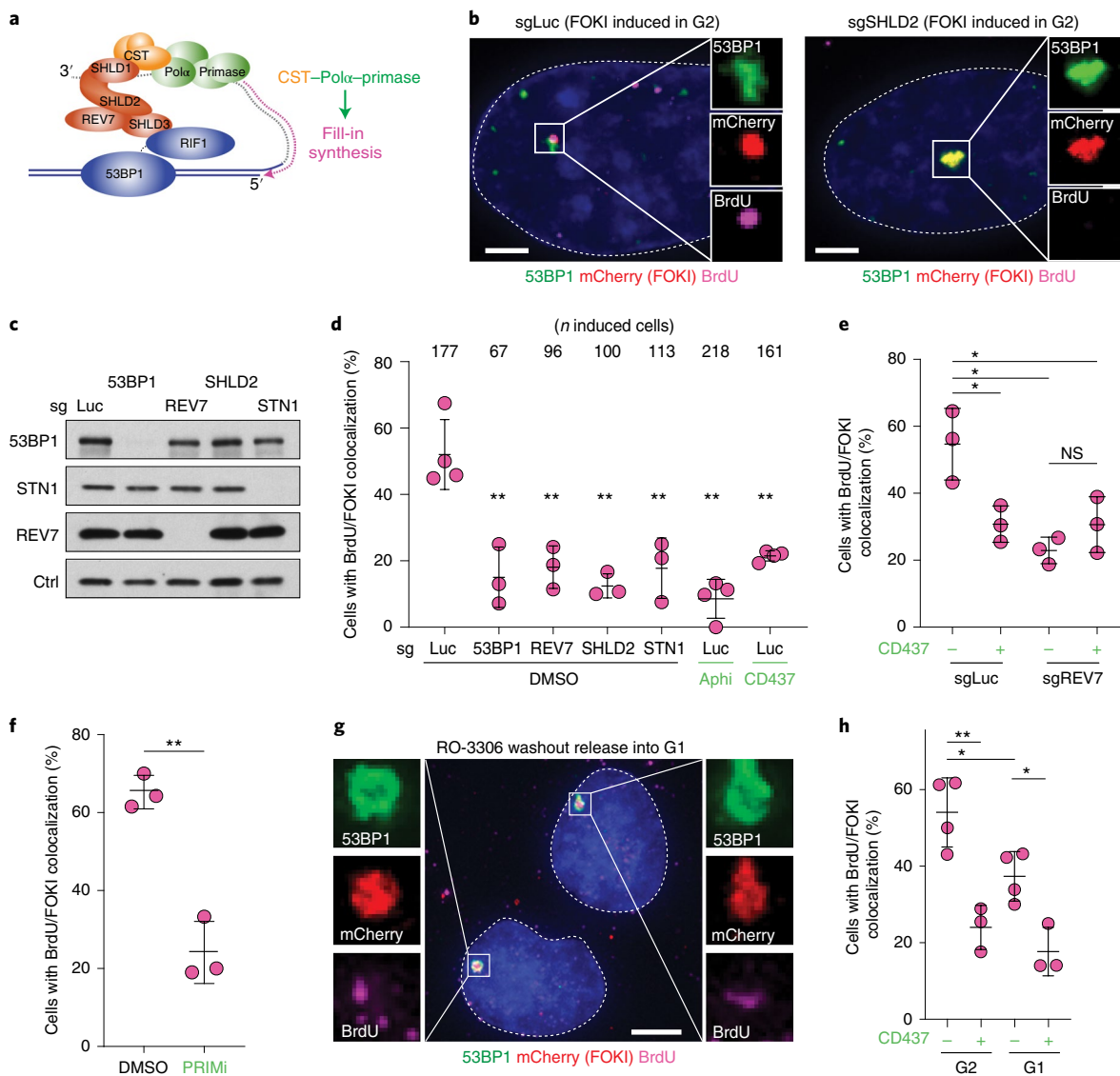
Fig. 2 | 53BP1–shieldin–CST–Polα–primase-dependent fill-in synthesis at FOKI-induced DSBs. a, Schematic of the fill-in synthesis model. Shieldin recruits the CST complex and Polα–primase to counteract resection by copying the 3′ overhang. **b**, Representative IF images of U2OS-FOKI-LacI cells with control (sgLuc; left) or SHLD2 (sgSHLD2; right) CRISPR KO, in which FOK1 cutting has been induced. Cells were arrested in G2 with RO-3306 (9 μM overnight). Scale bars, 5 μm. Images representative of three independent experiments. **c**, Immunoblots showing bulk CRISPR-mediated disruption of the indicated 53BP1 pathway components. No validated antibody to SHLD2 is available. Ctrl, nonspecific band from REV7 blot. Image representative of two independent experiments. **d**, Quantification of BrdU colocalization with FOKI-induced DSBs, as in **b** and **c**, in cells treated with the indicated bulk CRISPR and dimethylsulfoxide (DMSO) or Polα inhibitors aphidicolin (Aphi) or CD437. n = three or four independent experiments as indicated. S-phase cells, identified based on BrdU labelling pattern, were excluded (for a sample image, see Extended Data Fig. 3b). **e**, Quantification of BrdU colocalization with FOKI-induced DSBs, as in **d**, to determine epistasis of REV7 KO and Polα inhibition. **f**, Quantification of BrdU colocalization with FOKI-induced DSBs, as in **d**, after inhibition of primase (PRIMi) with vidarabine triphosphate. In **e** and **f**, n = three independent experiments. **g**, Representative IF image of U2OS cells with FOKI-induced DSB in G2-arrested cells (9 μM RO-3306 overnight) or cells released from RO-3306 into G1 (2 h washout before induction of FOKI, see also Extended Data Fig. 3c). Scale bar, 5 μm. **h**, Quantification of BrdU colocalization with FOKI-induced DSBs, as in **g**, with or without Polα inhibition (CD437). n = three (CD437+) or four (CD437-) independent experiments. Statistical analyses as in Fig. 1. All means are indicated with centre bars and s.d. with error bars.

primase, like CST–Polα, contributes to the processing of DSBs in BRCA1-deficient cells.

Direct evidence for shieldin–CST–Polα–primase-dependent fill-in synthesis. A prediction of the fill-in model is that nucleotides are incorporated at DSBs (Fig. 2a). To test this prediction, we used the inducible mCherry–FOKI–LacI nuclease targeting a LacO array in U2OS cells[26]. Using this system, we previously observed recruitment of CST and Polα to DSBs in G2-arrested cells[19]. Incubation with BrdU during DSB induction in G2-arrested cells (Extended Data Fig. 3a) followed by denaturation and immunofluorescence (IF) imaging for BrdU revealed the incorporation of nucleotides at DSBs marked by mCherry–FOKI and 53BP1 (Fig. 2b). S phase cells were easily distinguished by their global BrdU incorporation and were excluded from this analysis (Extended Data Fig. 3b). The incorporation of BrdU at DSBs depended on the 53BP1–shieldin–CST–Polα axis (Fig. 2c,d), as revealed by CRISPR bulk targeting or inhibition of Polα by aphidicolin (a B-family polymerase inhibitor)
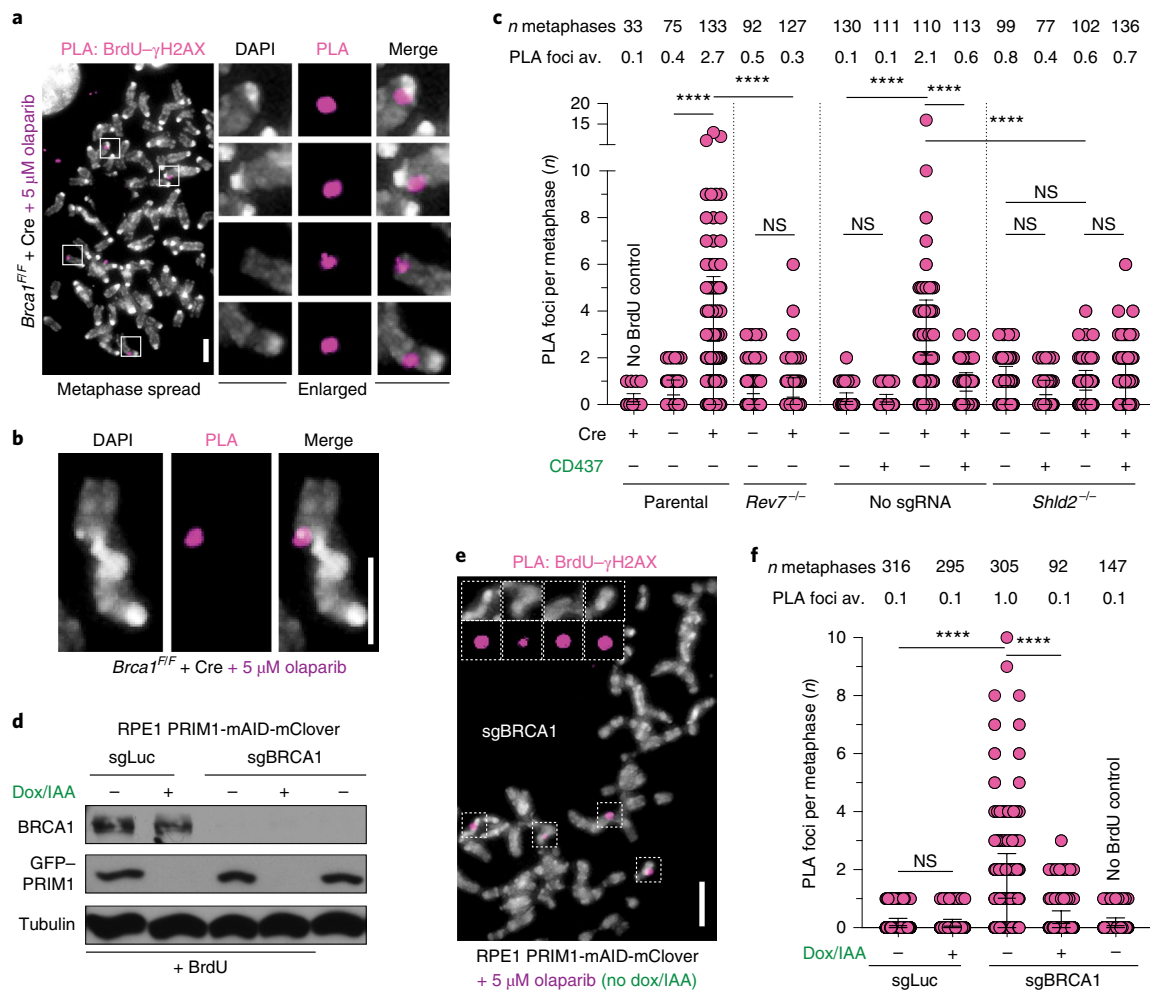
Fig. 3 | Detection of shieldin-dependent fill-in synthesis in BRCA1-deficient cells. a, Representative image from metaPLA of BrdU–γH2AX on metaphase spreads in *Brca1*[F/F] MEFs treated as indicated. **b**, Example of a dicentric chromosome from a metaphase spread showing a PLA signal at a break. **c**, Quantification of BrdU–γH2AX metaPLA foci at chromatin breaks, as in **a**, from cells with the indicated genotypes and treatments. The number of metaphases analysed per condition (*n*) and the average (av.) number of PLA foci at breaks per metaphase are indicated. **d**, Immunoblots for BRCA1 and GFP (mClover-PRIM1) in the indicated cells lines. **a–d** are representative of three independent experiments. **e**, Representative image from metaPLA of BrdU–γH2AX on metaphase spreads in RPE1 PRIM1-mAID-mClover cells treated with sgBRCA1, BrdU and olaparib. **f**, Quantification of BrdU–γH2AX metaPLA foci at chromatin breaks in cells, as in **d**, with the indicated genotypes and treatments. Data and representative image from three independent experiments. Number of metaphases analysed per condition (*n*) and the average number of PLA foci at breaks per metaphase are indicated. Statistical analyses as in Fig. 1, except in **c**, where ordinary one-way analysis of variance (ANOVA) with Tukey's multiple comparisons test was used. *P* values are as in Fig. 1. All means are indicated with centre bars and s.d. with error bars. All scale bars, 5 μm.

or CD437 (a specific Polα inhibitor[27]). Polα inhibition did not further reduce BrdU incorporation when REV7 was targeted (Fig. 2e), which is consistent with the notion that BrdU incorporation reflects 53BP1–shieldin–CST-dependent fill-in synthesis by Polα. In addition, treatment with a selective inhibitor of primase, vidarabine triphosphate[28], strongly reduced BrdU incorporation at FOKI-induced DSBs (Fig. 2f).

Although global BrdU incorporation during DNA synthesis prevents testing whether fill-in synthesis occurs at DSBs in S phase, we tested whether it could occur in G1. HA-tagged STN1 (HA–STN1) localized to FOKI-induced DSBs in cells released from cyclin-dependent kinase inhibition (CDKi) into G1 (Extended Data Fig. 3c–e). Cells released into G1—but not yet displaying the BrdU pattern of S phase cells—showed BrdU enrichment at FOKI-induced DSBs in a Polα-dependent manner (Extended Data Fig. 3c and Fig. 2g,h). The level of incorporation of BrdU at DSBs in this G1-enriched population was slightly lower than in G2-arrested cells (Fig. 2h). Analysis of cyclin A-negative cells revealed that a

majority of G1 cells displayed BrdU and FOKI colocalizations, and this BrdU incorporation was suppressed by treatment with CD437 (Extended Data Fig. 3f,g). Given the strong suppression of fill-in in G1 by CD437, we infer that some of the residual BrdU signal in G2-arrested cells treated with CD437 (Fig. 2c) is probably due to other DNA repair pathways (for example, HDR) that are inactive in G1.

We next aimed to detect BrdU incorporation at chromosome breaks in metaphase spreads of BRCA1-deficient, PARPi-treated cells. To this end, we combined a protocol for γH2AX IF on metaphase spreads[29–31] with PLA for detecting γH2AX and BrdU antibodies in close proximity (<40 nm). To test this metaPLA protocol, we used the induction of γH2AX foci at dysfunctional telomeres in mouse embryo fibroblasts (MEFs) deficient in both TRF2 (also known as TERF2) and ligase 4 (*Trf2*[F/F]*Lig4*^{−/−} MEFs treated with Cre)[32]. After BrdU incubation for 24 h to label all DNA, numerous BrdU–γH2AX PLA foci were observed at chromosome ends (Extended Data Fig. 4a,b), which demonstrates that this assay is

specific for sites of DNA damage and does not yield false-positive signals in MEFs.

To monitor fill-in at DSBs in PARPi-treated BRCA1-deficient cells, metaphases were collected after a short pulse (1 h) of BrdU, thereby avoiding confounding signals derived from S-phase cells. BRCA1-deficient PARPi-treated metaphase spreads showed BrdU–γH2AX PLA foci colocalizing with 4,6-diamidino-2-phenylindole (DAPI)-stained chromosomal material (Fig. 3a and Extended Data Fig. 4c). The presence of PLA foci depended on the PARPi dose, BrdU, primary antibodies and PLA probes (Extended Data Fig. 4d,e). Many PLA foci colocalized with gaps in DAPI staining or were present at the ends of broken chromosomes (Fig. 3a,b). BrdU–γH2AX metaPLA foci did not form in cells lacking REV7 or SHLD2 or when Polα was inhibited (Fig. 3c and Extended Data Fig. 4c,d). Similarly, BrdU–γH2AX metaPLA foci at breaks and gaps were eliminated by auxin-mediated degradation of primase in human cells (Fig. 3d–f). These results indicate that shieldin and its downstream effectors CST–Polα–primase mediate the incorporation of nucleotides at FOKI- and PARPi-induced DSBs.

The incorporation of BrdU at chromosome breaks in the 1 h time interval before metaphase indicated that fill-in synthesis occurs in late G2 or early M. Consistent with this finding, Polα inhibition after CDKi removal significantly diminished the formation of radial chromosomes (Extended Data Fig. 5a,b). We next determined whether Polα acts before or after nuclear envelope (NE) breakdown, which reaches a plateau at 30 min after release from CDKi as did the formation of RAD51 foci in cells treated with CD437 (Extended Data Fig. 5c–e). This result suggests that most cells that exit G2 arrest in this protocol do so within 30 min after release from CDKi. Polα inhibition within this short window reduced radial chromosome formation, while Polα inhibition after NE breakdown had no effect on radial chromosome formation (Extended Data Fig. 5f), which indicates that the Polα-dependent DNA repair steps take place in G2 immediately before or during NE breakdown, but not after.

Tethering of CST to DSBs can bypass the requirement for 53BP1–shieldin in BRCA1-deficient cells. It was previously shown that targeting human SHLD2 to DSBs using the forkhead-associated (FHA) domain of RNF8 (which targets proteins to phosphorylated MDC1 at DSBs) can bypass the need for recruitment of shieldin by 53BP1[22]. We first confirmed that tethered shieldin can function in the absence of 53BP1 in BRCA1-deficient MEFs (Fig. 4a). As expected, FHA-tethering of SHLD1 induced radial formation in cells deficient in both BRCA1 and 53BP1, and this effect was abolished when the FHA domain was mutated (R61Q) to abrogate the interaction with MDC1 (Fig. 4b and Extended Data Fig. 6a). Strikingly, Polα inhibition completely reversed the radial chromosomes induced by FHA–SHLD1 (Fig. 4c and Extended Data Fig. 6b).

Next, we tested whether CST could promote radial formation in BRCA1-deficient cells independently of 53BP1–shieldin. The expression of FHA–STN1, which localized to DSBs (Fig. 4d and

Extended Data Fig. 6c,d), restored radial formation in PARPi-treated *Brca1⁻/⁻53bp1⁻/⁻* and *Brca1⁻/⁻Shld2⁻/⁻* clones, which indicates that CST can function independently of 53BP1 and shieldin (Fig. 4e,f and Extended Data Fig. 6e). FHA–STN1 also increased the sensitivity of these cells to PARPi and reduced RAD51 loading (Fig. 4g,h). Shieldin-independent radial formation by FHA–STN1 was fully dependent on Polα activity (Fig. 4i and Extended Data Fig. 6f). The frequency of radials induced by both FHA–STN1 and FHA–SHLD1 in these experiments was slightly lower than what is observed when the endogenous 53BP1, shieldin and CST were present (Fig. 4b,f). This may indicate that the FHA fusion proteins are impaired in their function and/or recruitment. Collectively, the FHA-tethering experiments show that CST–Polα–primase can promote DSB processing in the absence of 53BP1 and shieldin.

SHLD1 function in BRCA1-deficient cells requires its interaction with CTC1. To determine the importance of the shieldin–CST interaction in BRCA1-deficient cells, we used a yeast two-hybrid random mutagenesis screen to identify a SHLD1 mutant (SHLD1ΔLDLP or SHLD1Δ) with impaired CTC1 interaction (Extended Data Fig. 7 and Fig. 5a). SHLD1Δ was expressed at the same level as wild-type (WT) SHLD1, was recruited to IR-induced DSBs at equal levels and retained its interaction with the carboxy terminus of SHLD2[22], yet showed a diminished interaction with CTC1 by co-immunoprecipitation (Fig. 5b,c and Extended Data Fig. 8a–c). Importantly, SHLD1Δ was defective in the recruitment of CST to IR-induced DSBs (Fig. 5d and Extended Data Fig. 8d–f).

To test the role of the SHLD1–CTC1 interaction in BRCA1-deficient cells, SHLD1Δ was introduced into RPE1 cells with both *BRCA1* and *SHLD1* knocked out (*BRCA1/SHLD1* DKO cells). Whereas WT SHLD1 prevented RAD51 loading, SHLD1Δ failed to repress RAD51 foci formation (Fig. 5e and Extended Data Fig. 8g–i). Concordantly, WT SHLD1 induced radial chromosome formation and PARPi sensitivity, but SHLD1Δ did not (Fig. 5f,g and Extended Data Fig. 8i). Furthermore, whereas FHA-tagged SHLD1 induced radial chromosomes in *Brca1⁻/⁻53bp1⁻/⁻* cells treated with PARPi (Fig. 4b,c), FHA-tagged SHLD1Δ was completely deficient in promoting radials in this setting (Fig. 5h,i).

To verify that the defect of SHLD1Δ in BRCA1-deficient cells is solely in the recruitment of CTC1, the interaction between CTC1 and SHLD1Δ was restored through a SNAP–HALO chemical-induced dimerization system[33] (Fig. 5j). Addition of the chemical dimerizer HaXS8 fully restored the ability of SHLD1Δ to suppress RAD51 loading in *BRCA1/SHLD1* DKO cells and rescued PARPi-induced radial chromosome formation (Fig. 5j–l). This result indicates that at DSBs in BRCA1-deficient cells, the primary function of SHLD1 is the recruitment of CTC1. The sufficiency of CST recruitment for radial formation (Fig. 4) combined with these SHLD1 separation of function studies supports a central role for CST–Polα–primase downstream of 53BP1–shieldin in BRCA1-deficient cells.

53BP1–shieldin also promotes CSR[18,20,34,35]. We therefore introduced SHLD1Δ into SHLD1-deficient CH12-F3 cells, a mouse

Fig. 4 | Bypass of 53BP1–shieldin by artificial tethering of CST. a, Schematic of 53BP1–shieldin-independent recruitment of FHA fusions to phosphorylated MDC1 at DSBs. **b**, Quantification of the percent of chromosomes involved in radial structures in the indicated cell lines with WT FHA–SHLD1 or FHA–SHLD1 with a FHA domain mutation (R61Q; RQ), which prohibits recruitment to DSBs. **c**, Quantification as in **b** in *Brca1^F/F^53bp1⁻/⁻* cells with or without FHA–SHLD1 and Polα inhibition (CD437). **d**, Representative image of irradiated *Brca1⁻/⁻Shld2⁻/⁻* cells harbouring eGFP–FHA–STN1, which colocalizes with 53BP1 IR-induced foci. The nucleus is demarcated by the dashed white line. Image representative of three independent experiments. Scale bar, 5 μm. **e**, Immunoblots for BRCA1, 53BP1, FHA–STN1 and STN1 in the indicated MEFs. Images representative of two independent experiments. **f**, Quantification as in **b** in the indicated cell lines with or without FHA–STN1. **g**, Quantification of colony formation by MEFs of the indicated genotype with or without FHA–STN1 and treated with 1 μM olaparib for 24 h. Survival after PARPi was compared to undrugged cells. Each dot represents one of three or four independent experiments. **h**, Quantification of the percent of RAD51-positive cells in irradiated MEFs of the indicated genotype with or without FHA–STN1. Each dot represents one of three or four independent experiments. **i**, Quantification of radial chromosome formation, as in **c**, in *Brca1^F/F^Shld2⁻/⁻* cells with or without FHA–STN1 and Polα inhibitor. In **b**, **c**, **f** and **i**, the number of metaphases (*n*, each represented by a dot) pooled from three independent experiments is indicated in the figure. Statistical analyses as in Fig. 1. All means are indicated with centre bars and s.d. with error bars.

B-cell lymphoma line that undergoes highly efficient IgM to IgA class switching after stimulation. Unexpectedly, expression of SHLD1Δ—or a large amino-terminal truncation of SHLD1 that includes the LDLP motif deleted in SHLD1Δ—restored CSR to the same extent as WT SHLD1 (Fig. 6a,b). In this context, no interaction was detected between immunoprecipitated WT SHLD1 or
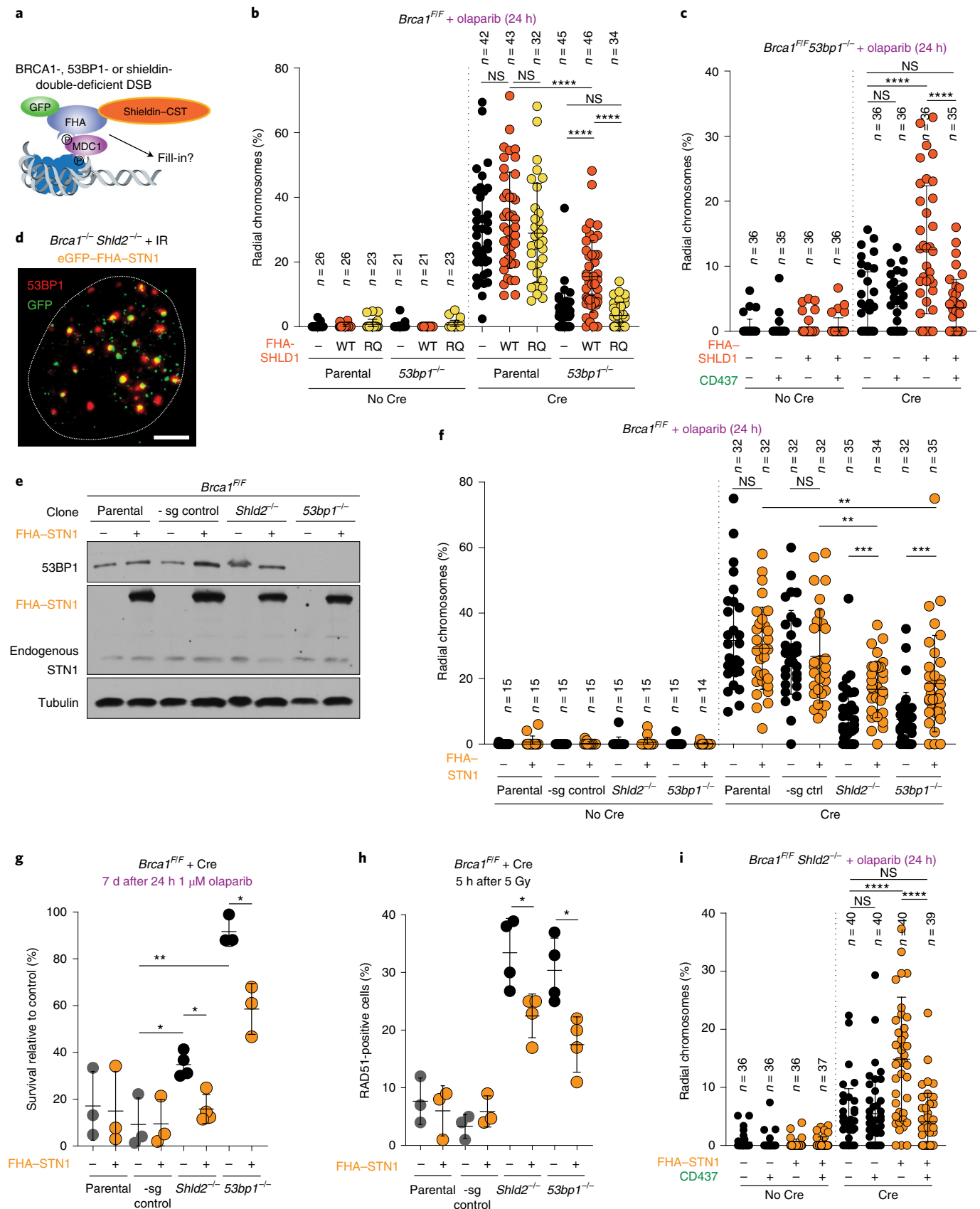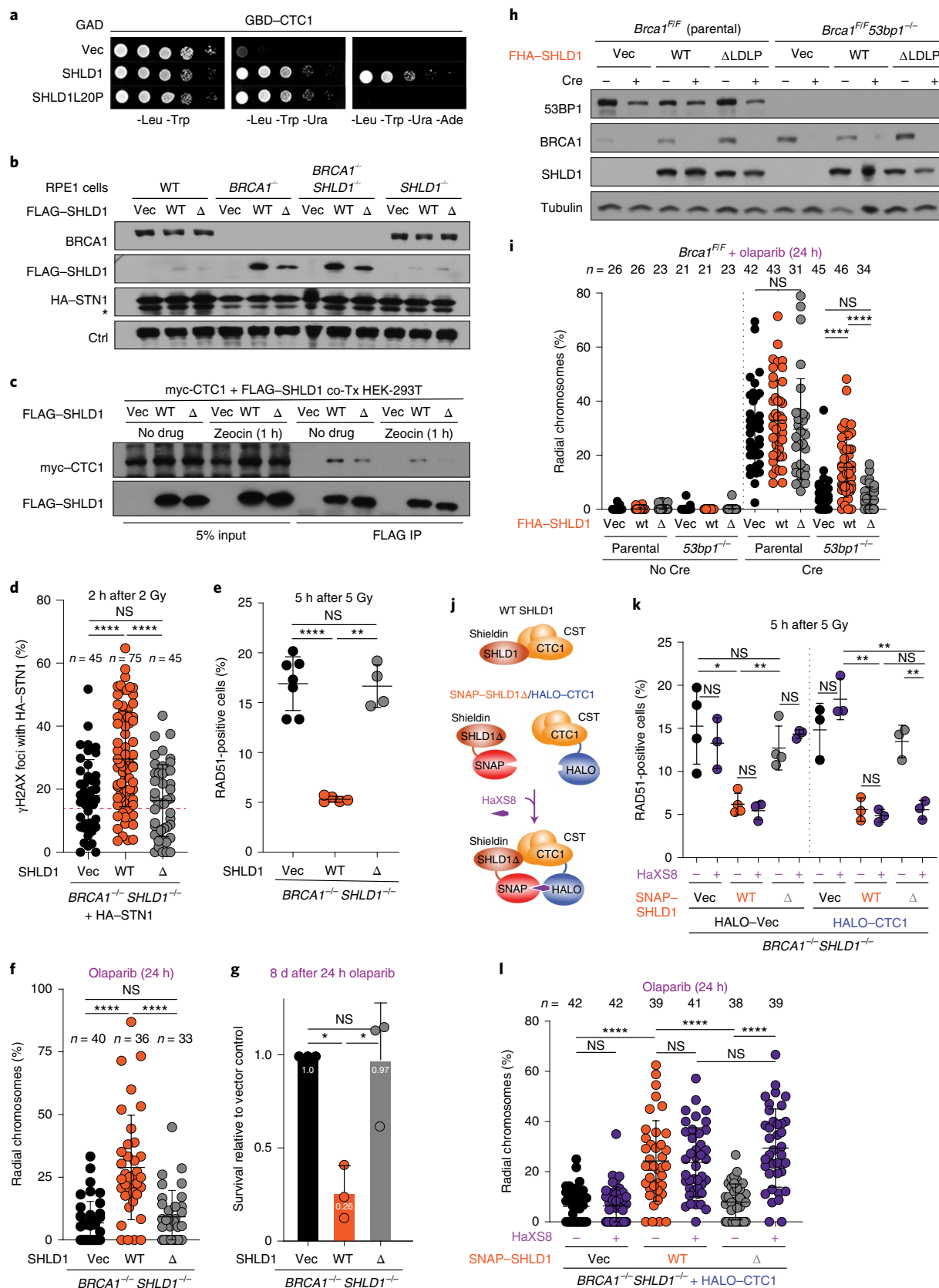
SHLD1Δ and CST (as judged by STN1 immunoblotting, as no validated antibody to mouse CTC1 is available) (Fig. 6c). Therefore, we have no information on whether the mutants abrogate the interaction of SHLD1 with CTC1 in these cells.

We next examined SHLD1Δ function at telomeres lacking the end protection afforded by shelterin[36], where 53BP1–shieldin–CST have been shown to counteract 5′ end resection[19]. As determined by a quantitative assay for changes in the relative amount of ss

Fig. 5 | Shieldin function in BRCA1-deficient cells depends on the SHLD1–CTC1 interaction. a, Yeast two-hybrid assay demonstrating the lack of interaction between human SHLD1L20P and CTC1 proteins. Colony growth on permissive (-leucine, -tryptophan, -uracil), but not selective (-leucine, -tryptophan, -uracil and -adenine) medium indicates lack of interaction. Vec, vector. **b**, Immunoblots in the indicated cells. SHLD1Δ (Δ) has a deletion of amino acids 18–21. Ctrl, nonspecific band from STN1 blot. **a** and **b** are representative of two independent experiments. **c**, Immunoprecipitation (IP) of FLAG–SHLD1 and immunoblot for myc-CTC1 co-expressed (co-Tx) in HEK-293T cells. Image representative of four independent experiments. **d**, Quantification of IR-induced γH2AX foci with HA–STN1 signal in *BRCA1/SHLD1* DKO cells as in **b**. The number of nuclei (*n*, each represented by a dot) pooled from three independent experiments is indicated. Red dotted line indicates the average background level due to randomly overlapping γH2AX and HA foci (Methods). **e**, Quantification of the percent of RAD51-positive cells in irradiated *BRCA1/SHLD1* DKO RPE1 cells complemented with the indicated FLAG–SHLD1 construct or an empty vector. Each dot represents an independent experiment (*n* = 4–7 experiments involving >60 cells each). **f**, Quantification of the percent of chromosomes in radial structures in cells as in **e**. The number of metaphase spreads (*n*, each represented by a dot) pooled from three independent experiments is indicated. **g**, Quantification of colony formation by *BRCA1/SHLD1* DKO cells, as in **e**, treated with 5 μM olaparib for 24 h. Survival after PARPi was compared to undrugged cells and normalized to empty vector. *n* = three independent experiments. **h**, Immunoblot for BRCA1, 53BP1 and SHLD1 detecting FHA-tagged SHLD1 in the indicated cells. Image representative of three independent experiments. **i**, Quantification of the percent of chromosomes in radial structures in the indicated MEFs expressing FHA–SHLD1Δ (Δ). Empty vector and FHA–SHLD1 (WT) conditions from Fig. 4b are provided again here. The number of metaphase spreads (*n*, each represented by a dot) pooled from three independent experiments is indicated. **j**, Schematic of HaXS8-induced dimerization of SNAP–SHLD1Δ with HALO–CTC1. **k**, Quantification of RAD51-positive cells in irradiated *BRCA1/SHLD1* DKO cells, complemented with the indicated SNAP–SHLD1 or empty vector, and HALO–CTC1 or empty vector, then treated with HaXS8 or vehicle before irradiation. *n* = 3 or 4 independent experiments as indicated. **l**, Quantification of the percent of chromosomes in radial structures in *BRCA1/SHLD1 DKO* cells with the indicated treatments. The number of metaphase spreads (*n*, each represented by a dot) pooled from three independent experiments is indicated. Statistical analyses as in Fig. 1. All means are indicated with centre bars and s.d. with error bars.

telomeric DNA, deletion of the shelterin subunit TPP1 from *Tpp1^{F/F}Shld1^{−/−}* MEFs induced a greater 3′ overhang signal compared to deletion of TPP1 from SHLD1-proficient cells (Fig. 6d–f). As was the case for CSR, SHLD1Δ appeared to behave like WT SHLD1, in that it suppressed the increase in the 3′ overhang signal to the same extent (Fig. 6e,f). SHLD1Δ was expressed at the same level as WT SHLD1 and did not affect the expression of other proteins relevant to 53BP1 function (Fig. 6d and Extended Data Fig. 9a). Next, we tested whether the SHLD1 LDLP motif has a function that is specific to the BRCA1-deficient context. We used CRISPR to target *Brca1* in *Tpp1^{F/F}Shld1^{−/−}* MEFs and complemented them with WT SHLD1 or SHLD1Δ. However, deletion of BRCA1 did not alter the ability of SHLD1Δ to behave like WT SHLD1 in TPP1-deficient MEFs (Extended Data Fig. 9b,c). As was the case for the B cells used for CSR, we were unable to verify that the shieldin–CST interaction was diminished in MEFs that express SHLD1Δ (Extended Data Fig. 9d).

We tested the possibility that ATM signalling (as presumably elicited by DSBs in PARPi-treated BRCA1-deficient cells) affects the shieldin–CST interaction. Deletion of TPP1 results in activation of ATR signalling, whereas ATM signalling is activated at telomeres when the shelterin subunit TRF2 is deleted[36]. At telomeres lacking TRF2, both 53BP1 and REV7 repress the formation of excessive ss 3′ telomeric DNA, although the phenotype is not as strong as when TPP1 is absent[19,37]. Therefore, we used *Trf2^{F/F}Shld1^{−/−}* MEFs to compare the effect of SHLD1Δ and WT SHLD1 on the formation of excessive ss telomeric DNA. The MEFs also lacked ligase 4, thereby avoiding the confounding effect of telomere fusion after TRF2 deletion. In this context, SHLD1Δ repressed the 3′ telomeric overhang phenotype in a comparable manner to WT SHLD1 (Extended Data Fig. 10a–c). This finding held even when BRCA1 was co-deleted from the cells (Extended Data Fig. 10d,e). Thus, the SHLD1Δ mutant behaves differently in the context of dysfunctional telomeres and CSR than at the random DSBs in the BRCA1-deficient cells studied above. A possible reason for this distinction is discussed below.

Discussion

Determining how the RIF1–shieldin axis of 53BP1 prevents long 3′ overhangs in DSB repair has been a subject of intensive research. Recently, two (non-mutually exclusive) models arose: 5′ end resection is blocked or resection is counteracted by fill-in synthesis. The data presented here provide direct evidence for the fill-in reaction in BRCA1-proficient and BRCA1-deficient cells in the form of incorporation of nucleotides at nuclease- or PARPi-induced DSBs in a 53BP1–shieldin–CST–Polα–primase-dependent manner (Figs. 2 and 3). We also highlighted the critical role of fill-in synthesis in BRCA1-deficient cells. In this setting, we showed the involvement of primase in promoting radial chromosomes (Fig. 1), the ability of DSB-tethered CST to bypass the need for 53BP1–shieldin (Fig. 4), and, based on a SHLD1 mutant (SHLD1Δ) that lacks CST binding, the requirement of CST recruitment for the function of shieldin in suppressing RAD51 loading and promoting radial formation (Fig. 5). These hallmarks of shieldin loss in BRCA1-deficient cells were reversed when CST was force-tethered to shieldin containing SHLD1Δ by chemical-induced dimerization. Collectively, the data argue that shieldin function in BRCA1-deficient cells requires the interaction of shieldin with CST.

Fig. 6 | SHLD1Δ supports CSR and suppresses long telomeric overhang formation. a, Representative flow cytometry plots of IgM to IgA CSR in indicated parental *Shld1^{+/+}*, *Shld1^{−/−}* and transgene-complemented CH12-F3 cell line derivatives. Images representative of three independent experiments. **b**, Quantification of CSR in cells as in **a**. CSR efficiency is normalized to WT cells. Statistical analysis (*n* = 3 independent experiments) performed using ordinary one-way ANOVA with Dunnett's correction for multiple comparisons. All comparisons are made to *Shld1^{−/−}* cells complemented with WT SHLD1. **c**, TwinStrep-HA–SHLD1 WT, L20P, ΔLDLP or ΔN immunocomplexes were isolated from whole cell extracts prepared from untreated CH12-F3 cultures. Western blots were probed for the indicated targets. Data represent three independent experiments. **d**, Immunoblot showing CHK1 activation after *Tpp1* deletion and SHLD1 construct expression in the indicated cells. Images representative of two independent experiments. **e**, Quantitative analysis of telomeric ss overhang intensity in cells as in **d** using in-gel hybridization to detect the 3′ overhang followed by rehybridization to the denatured DNA in the same gel, allowing the ratio of ss to total TTAGGG signal to be determined. Results representative of three independent experiments. **f**, Quantification of overhang intensity from cells as in **e** in *n* = 2 (*Shld1^{+/+}*) or 3 (*Shld1^{−/−}*) independent experiments using two independent clones for each genotype (represented by circle and square, diamond and hexagon symbols). Statistical analysis was performed using two-tailed ratio-paired *t*-test. Ref, reference sample. *P < 0.05, **P < 0.01, ****P < 0.0001. All means are indicated with centre bars and s.d. with error bars.

CST has been implicated both in CSR and at dysfunctional telomeres[19,35], two systems that have been extensively used as surrogates for DSB processing. Our previous work showed that shieldin recruits CST to dysfunctional telomeres and that shieldin and CST are epistatic in their control of excessive 3′ ss telomeric DNA[19]. Yet, the SHLD1Δ mutant that does not bind CTC1 was fully

functional in promoting CSR and preventing excessive ss 3′ overhangs at dysfunctional telomeres. The difference in function of SHLD1Δ at random DSBs in BRCA1-deficient cells and at DNA ends in CSR and at dysfunctional telomeres was not due to the presence of BRCA1 in the cells nor was it related to the activation of ATM versus ATR signalling.
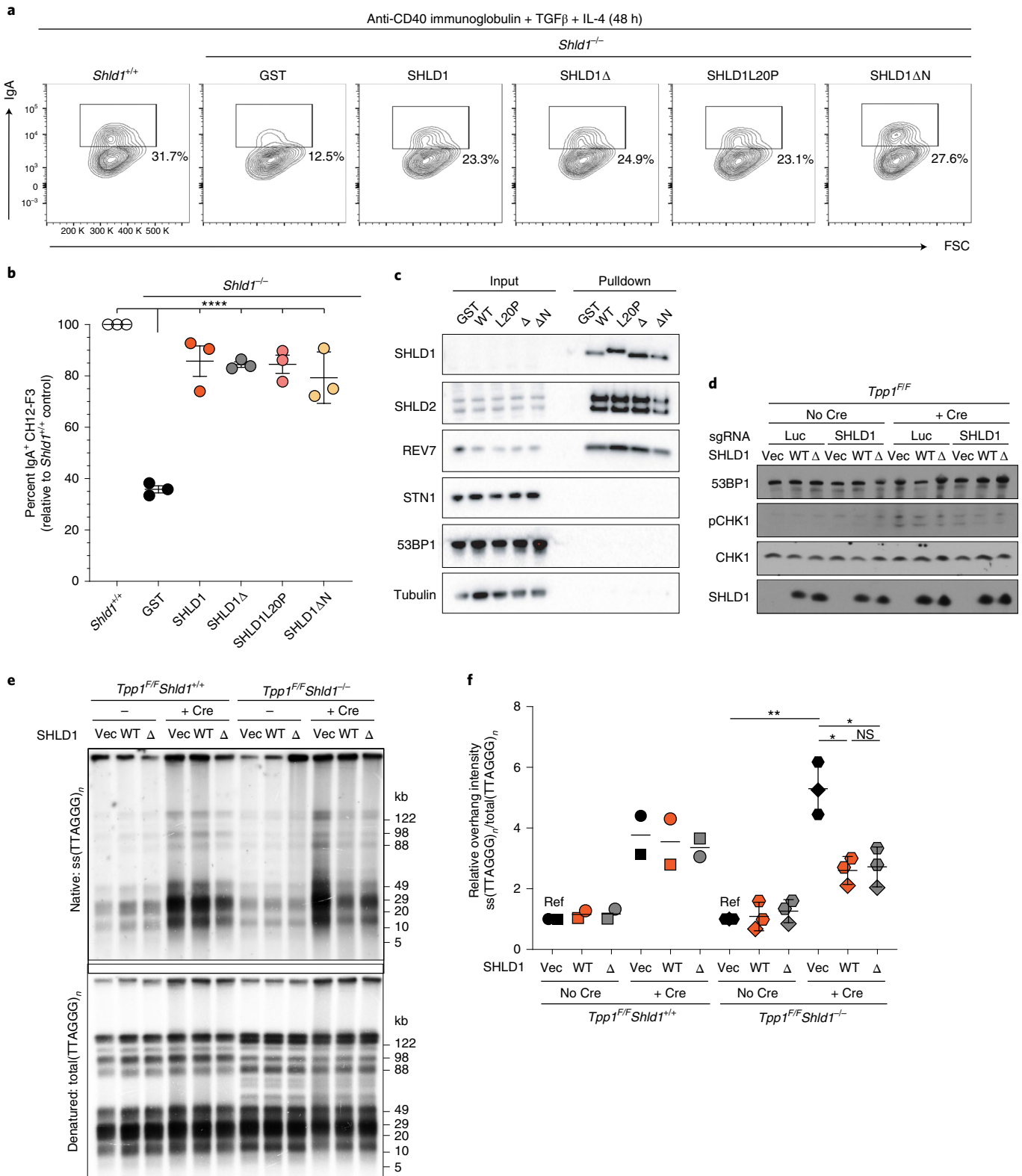
What might account for the discordant behaviour of SHLD1Δ? It is possible that SHLD1Δ behaves differently in CSR and at dysfunctional telomeres versus random DSBs due to a difference in cell-cycle phase of repair events, cell type (B cells for CSR) or chromatin context. However, we favour the explanation that SHLD1Δ is less deleterious to CST recruitment at DNA ends that bear CST recognition sites. The preferred substrates of CST are tandem repeats that contain runs of three or more G residues (for example, TTAGGG), but it also binds ssDNA containing multiple copies of GG dinucleotides[38]. The DNA ends formed during CSR have many tandem G-rich repeats[39], and the TTAGGG repeats of telomeres represent the optimal CST binding site. In particular, the mouse IgA switch region studied here contains more than 60 copies of tandem 5 nucleotide repeats containing GG or GGG (Extended Data Fig. 10f), and it is likely that these repeats can be bound by CST. The presence of these CST binding sites, together with the additional interactions between STN1 and TEN1 in CST and SHLD2, SHLD3 and REV7 in shieldin[19], may make up for the lack of CTC1–SHLD1 interaction in the context of SHLD1Δ. In contrast, repeated runs of G residues will be less frequent at many of the random DNA ends created by IR or PARPi, thereby diminishing the CST–DNA interaction and making CST more reliant on its binding to SHLD1. We therefore propose that the behaviour of SHLD1Δ in CSR and at dysfunctional telomeres represents an exception rather than the norm.

This idea that shieldin is important to facilitate the association of CST with DNA ends that lack preferred CST binding sites is consistent with the results of our bypass experiments in which tethering of FHA–STN1 to DSBs did not fully complement the loss of SHLD2 (Fig. 4f–h). Although this finding could be due to suboptimal function and/or recruitment of FHA fusion proteins, it is also possible that the shieldin–CST interaction improves the binding of CST to A-T rich overhangs, perhaps allowing CST to compete with RPA despite its lower affinity[38]. The in vitro binding affinity of SHLD2-C–SHLD1 (10 nM) is low compared to RPA[22], but the binding affinity of a complex formed by shieldin and CST (while undetermined) is likely to be much higher. It will be of interest to study the biochemistry and structural biology of CST–Polα–primase in complex with shieldin bound to ssDNA with and without runs of G residues. We have previously suggested that shieldin might function analogously to shelterin, which uses its TPP1 and POT1 subunits to recruit CST to fully protected telomeres[36]. A comparison of CST in complex with shieldin and with TPP1–POT1 would therefore be particularly informative. Finally, mutations in CST are responsible for the rare developmental disorder Coats plus[40], and the impact of these mutations on DSB repair warrants analysis. We and others have raised the possibility that 53BP1 acts primarily to ensure the fidelity of DSB repair[1,41]. If so, the major outcome of inherited mutations that affect how shieldin and CST cooperate at DSB repair could be an increase in mutagenic repair and perhaps an associated increase in cancer risk.

While this manuscript was in revision, two reports[42,43] were published in support of the idea that fill-in synthesis is a general phenomenon at DSBs. A broad role for Polα-mediated fill-in at genome-wide DSBs was noted at CRISPR–Cas9-induced DSBs[42] and at DSBs induced by AsiSI[43]. These results are in keeping with our finding of CST–Polα–primase-dependent fill-in at FOKI-induced DSBs and further highlight the critical role of this mode of DSB processing.

Online content

Any methods, additional references, Nature Research reporting summaries, source data, extended data, supplementary information, acknowledgements, peer review information; details of author contributions and competing interests; and statements of data and code availability are available at https://doi.org/10.1038/s41556-021-00812-9.

References

1. Mirman, Z. & de Lange, T. 53BP1: a DSB escort. *Genes Dev.* **34**, 7–23 (2020).
2. Pannunzio, N. R., Watanabe, G. & Lieber, M. R. Nonhomologous DNA end-joining for repair of DNA double-strand breaks. *J. Biol. Chem.* **293**, 10512–10523 (2018).
3. Wright, W. D., Shah, S. S. & Heyer, W. D. Homologous recombination and the repair of DNA double-strand breaks. *J. Biol. Chem.* **293**, 10524–10535 (2018).
4. Hustedt, N. & Durocher, D. The control of DNA repair by the cell cycle. *Nat. Cell Biol.* **19**, 1–9 (2016).
5. Bhattacharyya, A., Ear, U. S., Koller, B. H., Weichselbaum, R. R. & Bishop, D. K. The breast cancer susceptibility gene *BRCA1* is required for subnuclear assembly of Rad51 and survival following treatment with the DNA cross-linking agent cisplatin. *J. Biol. Chem.* **275**, 23899–23903 (2000).
6. Farmer, H. et al. Targeting the DNA repair defect in BRCA mutant cells as a therapeutic strategy. *Nature* **434**, 917–921 (2005).
7. Roy, R., Chun, J. & Powell, S. N. BRCA1 and BRCA2: different roles in a common pathway of genome protection. *Nat. Rev. Cancer* **12**, 68–78 (2011).
8. Bouwman, P. et al. 53BP1 loss rescues BRCA1 deficiency and is associated with triple-negative and BRCA-mutated breast cancers. *Nat. Struct. Mol. Biol.* **17**, 688–695 (2010).
9. Bunting, S. F. et al. 53BP1 inhibits homologous recombination in Brca1-deficient cells by blocking resection of DNA breaks. *Cell* **141**, 243–254 (2010).
10. Setiaputra, D. & Durocher, D. Shieldin—the protector of DNA ends. *EMBO Rep.* **20**, e47560 (2019).
11. Zimmermann, M., Lottersberger, F., Buonomo, S. B., Sfeir, A. & de Lange, T. 53BP1 regulates DSB repair using Rif1 to control 5′ end resection. *Science* **339**, 700–704 (2013).
12. Escribano-Díaz, C. et al. A cell cycle-dependent regulatory circuit composed of 53BP1-RIF1 and BRCA1–CtIP controls DNA repair pathway choice. *Mol. Cell* **49**, 872–883 (2013).
13. Feng, L., Fong, K. W., Wang, J., Wang, W. & Chen, J. RIF1 counteracts BRCA1-mediated end resection during DNA repair. *J. Biol. Chem.* **288**, 11135–11143 (2013).
14. Chapman, J. R. et al. RIF1 is essential for 53BP1-dependent nonhomologous end joining and suppression of DNA double-strand break resection. *Mol. Cell* **49**, 858–871 (2013).
15. Di Virgilio, M. et al. Rif1 prevents resection of DNA breaks and promotes immunoglobulin class switching. *Science* **339**, 711–715 (2013).
16. Boersma, V. et al. MAD2L2 controls DNA repair at telomeres and DNA breaks by inhibiting 5′ end resection. *Nature* **521**, 537–540 (2015).
17. Xu, G. et al. REV7 counteracts DNA double-strand break resection and affects PARP inhibition. *Nature* **521**, 541–544 (2015).
18. Ghezraoui, H. et al. 53BP1 cooperation with the REV7–shieldin complex underpins DNA structure-specific NHEJ. *Nature* **560**, 122–127 (2018).
19. Mirman, Z. et al. 53BP1–RIF1–shieldin counteracts DSB resection through CST- and Polα-dependent fill-in. *Nature* **560**, 112–116 (2018).
20. Gupta, R. et al. DNA repair network analysis reveals Shieldin as a key regulator of NHEJ and PARP inhibitor sensitivity. *Cell* **173**, 972–988.e23 (2018).
21. Dev, H. et al. Shieldin complex promotes DNA end-joining and counters homologous recombination in BRCA1-null cells. *Nat. Cell Biol.* **20**, 954–965 (2018).
22. Noordermeer, S. M. et al. The shieldin complex mediates 53BP1-dependent DNA repair. *Nature* **560**, 117–121 (2018).
23. Gao, S. et al. An OB-fold complex controls the repair pathways for DNA double-strand breaks. *Nat. Commun.* **9**, 3925 (2018).
24. Findlay, S. et al. SHLD2/FAM35A co-operates with REV7 to coordinate DNA double-strand break repair pathway choice. *EMBO J.* **37**, e100158 (2018).
25. Natsume, T., Kiyomitsu, T., Saga, Y. & Kanemaki, M. T. Rapid protein depletion in human cells by auxin-inducible degron tagging with short homology donors. *Cell Rep.* **15**, 210–218 (2016).
26. Tang, J. et al. Acetylation limits 53BP1 association with damaged chromatin to promote homologous recombination. *Nat. Struct. Mol. Biol.* **20**, 317–325 (2013).
27. Han, T. et al. The antitumor toxin CD437 is a direct inhibitor of DNA polymerase α. *Nat. Chem. Biol.* **12**, 511–515 (2016).
28. Holzer, S. et al. Structural basis for inhibition of human primase by arabinofuranosyl nucleoside analogues fludarabine and vidarabine. *ACS Chem. Biol.* **14**, 1904–1912 (2019).
29. Nakamura, A. et al. Techniques for gamma-H2AX detection. *Methods Enzymol.* **409**, 236–250 (2006).
30. Cesare, A. J. et al. Spontaneous occurrence of telomeric DNA damage response in the absence of chromosome fusions. *Nat. Struct. Mol. Biol.* **16**, 1244–1251 (2009).

31. Cesare, A. J., Heaphy, C. M. & O'Sullivan, R. J. Visualization of telomere integrity and function in vitro and in vivo using immunofluorescence techniques. *Curr. Protoc. Cytom.* **73**, 12.40.1–12.40.31 (2015).

32. Celli, G. B. & de Lange, T. DNA processing is not required for ATM-mediated telomere damage response after TRF2 deletion. *Nat. Cell Biol.* **7**, 712–718 (2005).

33. Erhart, D. et al. Chemical development of intracellular protein heterodimerizers. *Chem. Biol.* **20**, 549–557 (2013).

34. Franco, S. et al. H2AX prevents DNA breaks from progressing to chromosome breaks and translocations. *Mol. Cell* **21**, 201–214 (2006).

35. Barazas, M. et al. The CST complex mediates end protection at double-strand breaks and promotes PARP inhibitor sensitivity in BRCA1-deficient Cells. *Cell Rep.* **23**, 2107–2118 (2018).

36. de Lange, T. Shelterin-mediated telomere protection. *Annu. Rev. Genet.* **52**, 223–247 (2018).

37. Lottersberger, F., Bothmer, A., Robbiani, D. F., Nussenzweig, M. C. & de Lange, T. Role of 53BP1 oligomerization in regulating double-strand break repair. *Proc. Natl Acad. Sci. USA* **110**, 2146–2151 (2013).

38. Hom, R. A. & Wuttke, D. S. Human CST prefers G-rich but not necessarily telomeric sequences. *Biochemistry* **56**, 4210–4218 (2017).

39. Chaudhuri, J. & Alt, F. W. Class-switch recombination: interplay of transcription, DNA deamination and DNA repair. *Nat. Rev. Immunol.* **4**, 541–552 (2004).

40. Anderson, B. H. et al. Mutations in *CTC1*, encoding conserved telomere maintenance component 1, cause Coats plus. *Nat. Genet* **44**, 338–342 (2012).

41. Ochs, F. et al. 53BP1 fosters fidelity of homology-directed DNA repair. *Nat. Struct. Mol. Biol.* **23**, 714–721 (2016).

42. Schimmel, J., Muñoz-Subirana, N., Kool, H., van Schendel, R. & Tijsterman, M. Small tandem DNA duplications result from CST-guided Pol α-primase action at DNA break termini. *Nat. Commun.* **12**, 4843 (2021).

43. Paiano, J. et al. Role of 53BP1 in end protection and DNA synthesis at DNA breaks. *Genes Dev.* **35**, 19–20 (2021).

Methods

Cell culture and expression constructs. Immortalized $Brca1^{F/F}$, $Tpp1^{F/F}$ and $Trf2^{F/F}Lig4^{-/-}$ MEFs have been previously described[19,32,44]. MEFs were cultured in Dulbecco's modified Eagle medium (DMEM, Corning) supplemented with 15% fetal bovine serum (FBS; Gibco), non-essential amino acids (Gibco), 2 mM L-glutamine (Gibco), 100 U ml^{-1} penicillin, 100 μg ml^{-1} streptomycin (Gibco) and 50 μM β-mercaptoethanol (Sigma). Cre-mediated gene deletion experiments used retroviral infections with pMMP Hit&Run Cre three times[32]. Cells were collected 96 h after the second Cre infection unless otherwise indicated.

U2OS cells containing a LacO array and a tamoxifen- and Shield1-ligand-regulated mCherry–FOKI–LacI fusion were used as previously described[26] and cultured as described above. Cells were collected 4.5 h after induction of FOKI by the addition of 0.1 μM Shield1 and 10 μg ml^{-1} 4-hydroxytamoxifen. BrdU was added during FOKI induction, and S-phase cells displaying global BrdU incorporation were excluded from BrdU and FOKI colocalization analysis. When Polα inhibitors were used in the U2OS-FOKI cell line, they were added for 30 min before induction of FOKI and remained in the medium for the duration of DSB induction.

RPE1 cells were cultured in DMEM/F-12 medium (Gibco) supplemented with 10% FBS and penicillin–streptomycin as above. B-cell culture conditions for CSR experiments are described below. 293FT and Phoenix cells were cultured in DMEM supplemented with 10% bovine calf serum (BCS), non-essential amino acids, L-glutamine and penicillin–streptomycin as above.

Retroviral gene delivery was performed as previously described[45]. pWZL-GFP-FHA-mSTN1 and pWZL-GFP-mFHA-mSHLD1 were cloned using pENTR-eGFP-FHA-SHLD2C (ref. [22]) and pWZL-mSTN1 or pLPC-mSHLD1 (ref. [19]). For the purpose of complementation experiments, human SHLD1 plasmids were made single guide RNA (sgRNA)-resistant by site-directed mutagenesis of the target site TCAGCGTGTGACATAAGAGA changed to TCgGCcTGTGACATAAGAGA. Untagged mouse SHLD1 or SHLD1ΔLDLP was expressed from pWZL plasmids. WT mSHLD1 was made sgRNA-resistant by site-directed mutagenesis of the site TTGGATCTACCCGCGGTGTG changed to TTGGATCTACCCGCTGTGTG. Site-directed mutagenesis was also used to delete amino acids 18–21 (ΔLDLP) or to mutate the FHA domain (R61Q). Human STN1 tagged at the N-terminus with a 6×HA tag was delivered using the pLPC vector[19].

For co-immunoprecipitations, pCDNA5-FLAG-SHLD1 (ref. [19]) was modified by site-directed mutagenesis to delete amino acids 18–21 (ΔLDLP), and pLPC-myc-SHLD2C was generated by site-directed mutagenesis based on ref. [22]. pLPC-myc-CTC1 has been previously described[19]. These plasmids were used to clone pQCNeo-SNAP-SHLD1 and pLPC-Puro-HALO-CTC1, respectively, using Gibson assembly.

Drug treatments were as follows: olaparib (Selleck Chemicals): 1 μM unless otherwise noted; RO-3306 (Sigma): 9 μM; CD437 (Sigma): 10 μM; aphidicolin (Sigma): 2 μM; doxycycline (dox, Sigma): 2 μg ml^{-1}; IAA (auxin, 3-indole-acetic acid sodium salt dissolved in H$_2$O, Abcam): 500 μM; vidarabine triphosphate (Jena Biosciences): 10 μM; BrdU: 10 μM; zeocin (Invitrogen): 100 μg ml^{-1}. For chemical-induced dimerization, cells were treated with 0.5 μM HaXS8 (Tocris) 5 min before irradiation and collected 5 h later to examine RAD51 loading or 2 h before colcemid treatment for collection of metaphases.

CRISPR–Cas9 gene disruption. $Brca1^{F/F}$ $53bp1^{-/-}$ and $Brca1^{F/F}Rev7^{-/-}$ MEFs have been previously described[19]. $Brca1^{F/F}Shld2^{-/-}$ MEFs were generated by CRISPR–Cas9 targeting of exon 4 using the guide 5′-ATCAGTCAGATCCCTGCGTTCGG-(PAM)-3′. $Tpp1^{F/F}$ and $Trf2^{F/F}Lig4^{-/-}$ MEFs were targeted for Shld1 knockout using the guide 5′-CTGTACCTTGGATCTACCCG-(PAM)-3′. Human SHLD1 knockout RPE1 cells were generated by targeting exon 2 of SHLD1 using the guide 5′-TCTCTTATGTCACACGCTGA-(PAM)-3′ in BRCA1 KO $p53^{-/-}$ hTERT Cas9 RPE1 cells or an isogenic BRCA1-proficient control[22]. For all CRISPR-generated clones, biallelic gene disruption was verified by Sanger sequencing of Topo-cloned PCR products of the relevant locus (sequences available on request). Human 53BP1, REV7, SHLD2 and STN1 were targeted for bulk CRISPR KOs using the following sgRNAs in the lentiCRISPR v2 plasmid with selection in blasticidin: 53BP1-sgRNA1 (5′-CAGAATCATCCTCTAGAACC-(PAM)-3′), 53BP1-sgRNA2 (5′-TTGATCTCACTTGTGATTCG-(PAM)-3′), SHLD2-sgRNA1 (5′-TCTGGAGAACCAATAGATTC-(PAM)-3′), SHLD2-sgRNA2 (5′-TTTGAGCTAAAAAAGCAACC-(PAM)-3′), REV7-sgRNA1 (5′-CCTCAACTTTGGCCAAGGTA-(PAM)-3′), REV7-sgRNA2 (5′-TATACTGATTCAGCTCCGGG-(PAM)-3′), STN1-sgRNA1 (5′-GGCGGGACTCCTTCATGTCC(PAM)-3′), STN1-sgRNA2 (5′-GAGACCCCTTCCCTCTTGTG(PAM)-3′). Human BRCA1 and BRCA2 were targeted for bulk CRISPR KOs using the following sgRNAs in the lentiCRISPR v2 Puro plasmid (see experimental timeline). BRCA1-sgRNA (5′-GGCTCAGGGTTACCGAAGAG-(PAM)-3′). BRCA2-sgRNA1 (5′-GCAGGTTCAGAATTATAGGG-(PAM)-3′), BRCA2-sgRNA2 (5′-GTCTACCTGACCAATCGATG-(PAM)-3′) with 2 days selection in puromycin. For each gene, the two sgRNAs were either used individually or together. Mouse Brca1 exon 10 was targeted for bulk CRISPR KO using the guide (5′-GTATGCCAGAGAAAGCGGAG-(PAM)-3′).

For the generation of RPE1 PRIM1-mAID-mClover cells, p53- and RB-deficient RPE1-hTERT cells[46] were nucleofected with a donor template plasmid and two CRISPR–Cas9 plasmids targeting the last coding exon of PRIM1 (ref. [25]). Following selection in G418, mClover-positive cells were subcloned after flow-sorting for Clover and biallelically targeted clones were identified by PCR. HA-tagged OsTIR1 under the control of a dox-responsive promoter was introduced into PRIM1-AID-mClover clone 10 using lentiviral integration followed by selection in blasticidin and single-cell cloning. Eleven clones were picked and treated with 2 μg ml^{-1} dox for 24 h and collected for detection of HA-OsTIR1. Two clones expressing TIR1 at high levels were grown in the presence or absence of IAA and dox for 24 h and collected for immunoblotting. Efficient degradation of PRIM1-AID-mClover was seen in both clones. PRIM1 was completely degraded after 4 h treatment with 0.5 mM of IAA in both clones. Clone 9 was selected for future experiments. Gene targeting reagents were designed using Benchling.

Immunoblotting. Immunoblotting was performed as previously described[19] with the following antibodies: 53BP1 (175933, Abcam; 1:1,000; 100-304, Novus Biological; 1:1,000); BRCA1 (MAB22101, R&D Systems; 1:500); BRCA2 (OP95, Millipore; 1:500); CHK1 (8408, Santa Cruz; 1:1,000); pCHK1 (2341, Cell Signaling Technology; 1:1,000); CHK2 (611570, BD; 1:1,000); Flag-tag (M2, Sigma; 1:1,000); γ-tubulin (GTU488, Sigma; 1:20,000); GFP (11814460001, Sigma; 1:1,000); HA (3724, Cell Signaling Technology; 1:20,000); HSP70 (610608, BD; 1:1,000); MAD2L2/REV7 (180579, Abcam; 612266, BD; 1:1,000); Myc-tag (9B11, Cell Signaling Technology; 1:1,000); OBFC1/STN1 (89250, Abcam; 1:1,000; SC-376450, Santa Cruz; 1:1,000); PRIM1 (10773-1-AP, Proteintech; 1:1,000); RIF1 (1240, de Lange Lab; 1:1,000); SHLD1 (PA5-59280, ThermoFisher; 1:1,000); SNAP tag (9310, NEB; 1:1,000); TRF2 (1254, de Lange Lab; 1:5,000). Affinity-purified peptide antibodies against mouse SHLD1 and SHLD2 proteins (J.R.C., unpublished data; 1:1,000) were generated by Eurogentec.

Immunoprecipitation. Immunoprecipitation was carried out as previously described[19]. Co-transfection in 293FT cells was performed using calcium phosphate co-precipitation. Lysates were prepared in lysis buffer containing 50 mM Tris-HCl (pH 7.4), 300 mM NaCl, 10% glycerol, 0.1% NP-40, 1 mM PMSF, complete protease inhibitor without EDTA (Roche) and PhosSTOP phosphatase inhibitor mix (Roche). Samples were treated with 50 U Benzonase (Sigma) for 30 min at room temperature.

IF imaging. Previously published procedures were followed for IF imaging[45]. IF for BrdU (152095, Abcam; 1:500) with 53BP1 (612522, BD Biosciences; 1:1,000) or γH2AX (05636, Millipore; 1:1,000), HA-tagged STN1 (3724, Cell Signaling Technology; 1:5,000) or SNAP-tagged SHLD1 (9310, NEB; 1:1,000) was carried out using the cytoskeleton extraction protocol[47]. Cyclin A (611269, BD; 1:1,000) or lamin A/C (4200236, Sigma; 1:1,000) or γH2AX (05636, Millipore; 1:1,000) with RAD51 (70-001, Bioacademia; 1:1,000) were detected in cells fixed in 3% paraformaldehyde. Anti-mouse highly cross-absorbed Alexa Fluor plus 488 (1:500) and anti-rabbit highly cross-absorbed Alexa Fluor plus 647 (1:500) secondary antibodies were used (ThermoFisher). Imaging was performed on a DeltaVision (Applied Precision) equipped with a cooled charge-coupled device camera (DV Elite CMOS Camera), a PlanApo ×60, 1.42 NA objective (Olympus) and SoftWoRx software. For HA–STN1 and γH2AX colocalization, a random overlap background level was determined by splitting the two image channels, rotating one channel 90° and merging the channels. Colocalizations were then scored to determine the average overlap of foci by random chance due to telomeric (non-DSB) HA–STN1 foci or other spurious foci. For RAD51 foci studies, cells were considered RAD51 positive when the cell exhibited ten or more RAD51 foci colocalizing with 53BP1 or γH2AX foci. Image analysis was conducted using Fiji.

Metaphase chromosome analysis and PLA. Analysis of mis-rejoined chromosomes was carried out as described on DAPI-stained metaphase spreads after telomeric FISH[19]. The metaPLA protocol was developed based on a protocol for IF on metaphase spreads[29–31]. Cells were treated with BrdU for a total of 1 h (except where otherwise noted), during which colcemid was added for the final 45 min. For Polα inhibition, CD437 (10 μM) was added directly to the medium for 30 min before the addition of BrdU and kept in the medium during colcemid treatment. For metaPLA in RPE1 PRIM1-mAID cells, the experimental protocol in Fig. 1a was followed, with the addition of BrdU 15 min before washout. The PBS and FBS-containing medium used for washout contained BrdU, dox or IAA as appropriate, and cells were released into medium containing colcemid, BrdU, dox or IAA as appropriate for 50 min. Medium was then replaced with warm hypotonic buffer (10 mM Tris-HCl, 40 mM glycerol, 20 mM NaCl, 1 mM CaCl$_2$ and 0.5 mM MgCl$_2$) for 15 min at 37 °C. Cells were then collected by mitotic shakeoff and cytospinning (Shandon Cytospin3) for 10 min at 470g. Slides were immediately fixed in 2% paraformaldehyde in PBS. For metaPLA, cytospin spreads on glass slides were permeabilized in cold Triton X-100 buffer with 0.5% Triton[47] for 5 min, rinsed with H$_2$O, denatured in 1 N HCl for 10 min and rinsed again before proceeding with PLA. Mouse γH2AX (05636, Millipore; 1:1,000) and rabbit BrdU (152095, Abcam; 1:1,000) antibodies were used with minus and plus

probes and a Duolink Orange kit (Sigma). PLA foci were only scored at breaks, gaps or other aberrant chromosome structures. In $Trf2^{F/F}Lig4^{-/-}$ MEFs, only PLA foci at chromosome termini were scored. The number of PLA foci observed in $Trf2^{F/F}Lig4^{-/-}$ cells is consistent with not every dysfunctional telomere exhibiting a γH2AX focus in metaphase[48], and/or may reflect inefficiency in proximity labelling.

Yeast two-hybrid and SHLD1 mutagenesis screen. GBD–hCTC1 has been previously described[19] and was transformed into the budding yeast strain PJ69-4A (*MATa trp1-901 leu2-3,112 ura3-52 his3-200 gal4 gal80 LYS2::GAL1-HIS3 GAL2-ADE2 met2::GAL7-lacZ*) and selected on synthetic complete drop-out medium lacking tryptophan. To recover only full-length SHLD1 variants in the screen, GAD–hSHLD1[19] was modified to contain a C-terminal *ScUra3* gene. SHLD1 was then amplified by error-prone PCR (Taq, NEB) using the following conditions: 2.5 mM each dNTP; 7 mM MgCl$_2$; and 0.1 mM MnCl$_2$ in 10× buffer with MgCl$_2$. GAD–SHLD1WT-Ura3 was digested with Nde1/Age1 to remove the *SHLD1* open reading frame, and the linearized vector was co-transformed with the SHLD1 variant library at a molar ratio of 1 vector: 3 insert into yeast harbouring GBD–hCTC1 and plated on synthetic complete drop-out medium lacking tryptophan, leucine and uracil (SC-LTU). Colonies were then replica plated onto drop-out medium also lacking adenine (SC-LTUA). Colonies that failed to grow on selective (SC-LTUA) medium were picked from permissive medium, and spot dilutions were plated on selective and permissive media for validation. SHLD1 variant sequences were amplified by colony PCR, column purified and sequenced.

Survival assays. For PARPi survival assays, cells were seeded in 12-well or 6-well plates in duplicate. After 24 h, cells were treated with olaparib at the indicated concentrations for 24 h. Cells were then provided with medium without olaparib for the remainder of the experiment. Colonies were fixed and stained with 50% methanol, 2% methylene blue, rinsed with water and dried before counting. The survival percentage compared to untreated cells was calculated. Two technical replicates at two cell concentrations were scored for each condition in three independent experiments.

CSR assay. CH12-F3 cells and CRISPR–Cas9-edited *Shld1*$^{-/-}$ derivatives[18] were cultured in RPMI supplemented with 5% NCTC-109 medium, 10% FCS, 100 U ml^{-1} penicillin, 100 ng ml^{-1} streptomycin and 2 mM L-glutamine at 37 °C with 5% CO$_2$ under ambient oxygen conditions. Complemented cell lines were generated by lentivirus-mediated transduction, using viral supernatants collected from 293T cells co-transfected with third-generation packaging vectors and pLenti-PGK-PURO-DEST (Addgene, 19068) containing cloned transgene inserts. Typically, cells were spinoculated with polybrene (8 μg ml^{-1}) and HEPES (20 mM)-supplemented viral supernatants (480g, 90 min at 25 °C). Stable cell-lines were subsequently selected and maintained in the presence of puromycin (0.5 μg ml^{-1}). To stimulate CSR to IgA, CH12-F3 cells were stimulated with agonist anti-CD40 antibody (0.5 μg ml^{-1}; Miltenyi Biotec, FGK45.5), mouse IL-4 (5 ng μl^{-1}; R&D Systems) and TGFβ1 (2.5 ng μl^{-1}; R&D Systems). Cell-surface IgA expression was determined by flow cytometric staining with anti-mouse IgA–FITC antibody (ThermoFisher, 11-4204-82, MA-6E1). Pellets collected from cultures of ~4×10^7 CH12-F3 cells were lysed in BLB (Benzonase lysis buffer: 20 mM HEPES pH 7.9, 40 mM KCl, 2 mM MgCl$_2$, 10% glycerol, 0.5% NP40, 50 U ml^{-1} Benzonase (Novagen), 0.05% (v/v) phosphatase inhibitors (Sigma-Aldrich) and protease inhibitors (complete EDTA-free, Roche)) and were incubated on ice for 10 min before a second incubation with adjusted salt (450 mM KCl). TwinStrep-HA–SHLD1 WT, SHLD1ΔLDLP, L20P or ΔN complexes were isolated from clarified lysates, following their dilution in NSB (no-salt buffer: 20 mM HEPES (pH 7.9), 10% glycerol, 0.5 mM DTT, 0.5 mM EDTA, 0.05% (v/v) phosphatase inhibitors (Sigma-Aldrich) and protease inhibitors (Roche)) to a final salt concentration of 125 mM. Complexes were immunopurified on Strep-TactinXT-coated magnetic beads (IBA Life Sciences) and washed extensively in wash buffer (BLB supplemented with 125 mM KCl and 0.1% NP-40).

In-gel analysis of ss telomeric DNA. Mouse telomeric overhangs were analysed 96–120 h after Cre treatment by in-gel hybridization with a γ-^{32}P-ATP end-labelled [AACCCT]$_4$ probe as previously described[32]. After background subtraction, the signal from the native gel was compared to the signal from total telomeric DNA in the same lane obtained by rehybridization of the probe after in situ denaturation of the DNA in the gel. The ratios between ss/ds telomeric signals in each lane were then normalized to the ratio of vector control cells not treated with Cre.

Statistics and reproducibility. All statistical analyses and *P* values are described in the figure legends. No statistical methods were used to predetermine sample size. The sample size was determined based on previous, similar experiments in the laboratory. No data were excluded from the experiments presented in the study. All immunoblots and sample images are representative of at least three independent experiments (unless otherwise indicated) with similar results obtained. Our in vitro experiments are randomized as much as possible in the sense that culture dishes seeded with identical parental populations of cells were then chosen at random for the various biological perturbations. The investigators were not blinded to allocation during experiments and outcome assessment. Data were analysed using Microsoft Excel and Graphpad Prism.

Reporting Summary. Further information on research design is available in the Nature Research Reporting Summary linked to this article.

Data availability
All data that were generated and/or analysed in this study are included in the published paper and its Supplementary Information. Conservation symbols according to UniProt can be found at https://www.uniprot.org/. Source data are provided with this paper. All other data supporting the findings of this study are available from the corresponding author upon reasonable request.

References
44. Xu, X. et al. Centrosome amplification and a defective G2-M cell cycle checkpoint induce genetic instability in *BRCA1* exon 11 isoform-deficient cells. *Mol. Cell* **3**, 389–395 (1999).
45. Wu, P., Takai, H. & de Lange, T. Telomeric 3′ overhangs derive from resection by Exo1 and Apollo and fill-in by POT1b-associated CST. *Cell* **150**, 39–52 (2012).
46. Yang, Z., Maciejowski, J. & de Lange, T. Nuclear envelope rupture is enhanced by loss of p53 or Rb. *Mol. Cancer Res.* **15**, 1579–1586 (2017).
47. Mirzoeva, O. K. & Petrini, J. H. DNA damage-dependent nuclear dynamics of the Mre11 complex. *Mol. Cell Biol.* **21**, 281–288 (2001).
48. Cesare, A. J., Hayashi, M. T., Crabbe, L. & Karlseder, J. The telomere deprotection response is functionally distinct from the genomic DNA damage response. *Mol. Cell* **51**, 141–155 (2013).

Author contributions
Z.M. performed most of the experiments. N.K.S. designed and engineered the RPE1-PRIM1-AID cell line and performed some 3′ overhang assays. A.K. performed the CSR experiment under the supervision of J.R.C. Z.M. and T.d.L. conceived the study and wrote the manuscript with input from all authors.

Competing interests
T.d.L. is a member of the Scientific Advisory Board of Calico Life Sciences. The remaining authors declare no competing interests.
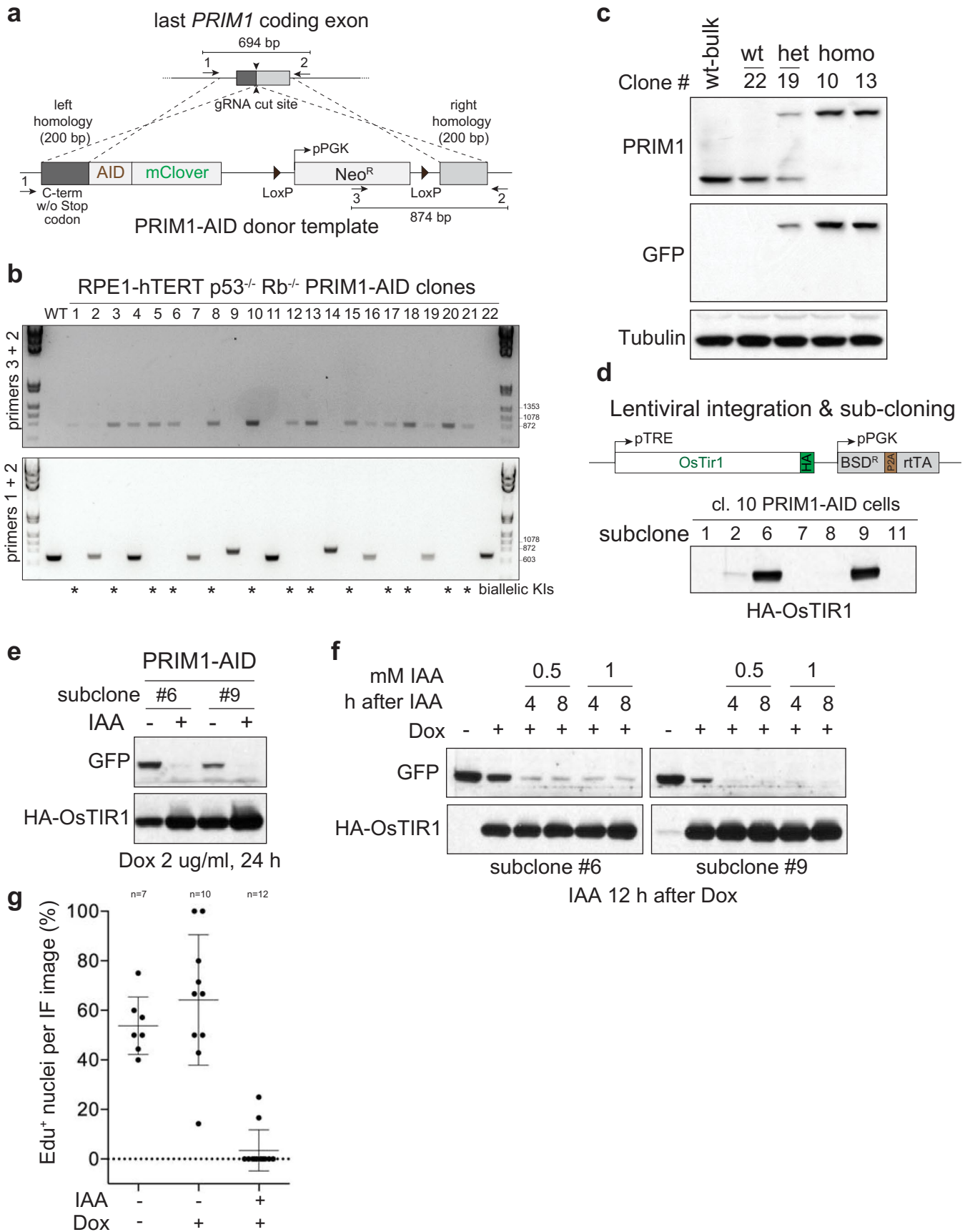
Additional information
Extended data is available for this paper at https://doi.org/10.1038/s41556-021-00812-9.

Supplementary information The online version contains supplementary material available at https://doi.org/10.1038/s41556-021-00812-9.

Correspondence and requests for materials should be addressed to Titia de Lange.

Peer review information *Nature Cell Biology* thanks the anonymous reviewers for their contribution to the peer review of this work.

Reprints and permissions information is available at www.nature.com/reprints.

a

last *PRIM1* coding exon

PRIM1-AID donor template

b

RPE1-hTERT p53$^{-/-}$ Rb$^{-/-}$ PRIM1-AID clones

* biallelic KIs

c

d

Lentiviral integration & sub-cloning

HA-OsTIR1

e

PRIM1-AID

Dox 2 ug/ml, 24 h

f

IAA 12 h after Dox

g

Extended Data Fig. 1 | See next page for caption.

Extended Data Fig. 1 | Generation and validation of p53/Rb-deficient RPE1 cells with mAID knocked into both PRIM1 loci (related to Fig. 1).
**a**, Experimental scheme used to tag endogenous PRIM1 with AID-mClover. **b**, PCR genotyping of mClover-positive clones. Location of primer sets and the expected PCR band sizes are shown in **a**. **c**, Immunoblot for mClover-PRIM1 with PRIM1 or anti-GFP antibody. Clone #10, with both copies of PRIM1 tagged with AID-mClover, was selected for the experiments. **d**, Schematic of HA-OsTIR1 and immunoblot confirming dox-induced HA-OsTIR1 in subclones of PRIM1-AID-mClover clone #10. **e**, Immunoblot for GFP showing efficient PRIM1 degradation after the indicated IAA (auxin)/dox treatments in two subclones. **f**, Immunoblot as in **e** but testing timing and concentration of IAA. **g**, IF showing loss of EdU incorporation in subclone #6 after auxin/dox-induced PRIM1-AID degradation indicating the expected inhibition of DNA replication. In **g**, the number of fields of view (n, each represented by a dot) is indicated. In **b-g**, the experiment has been performed once. Means are indicated with center bars and SDs with error bars.
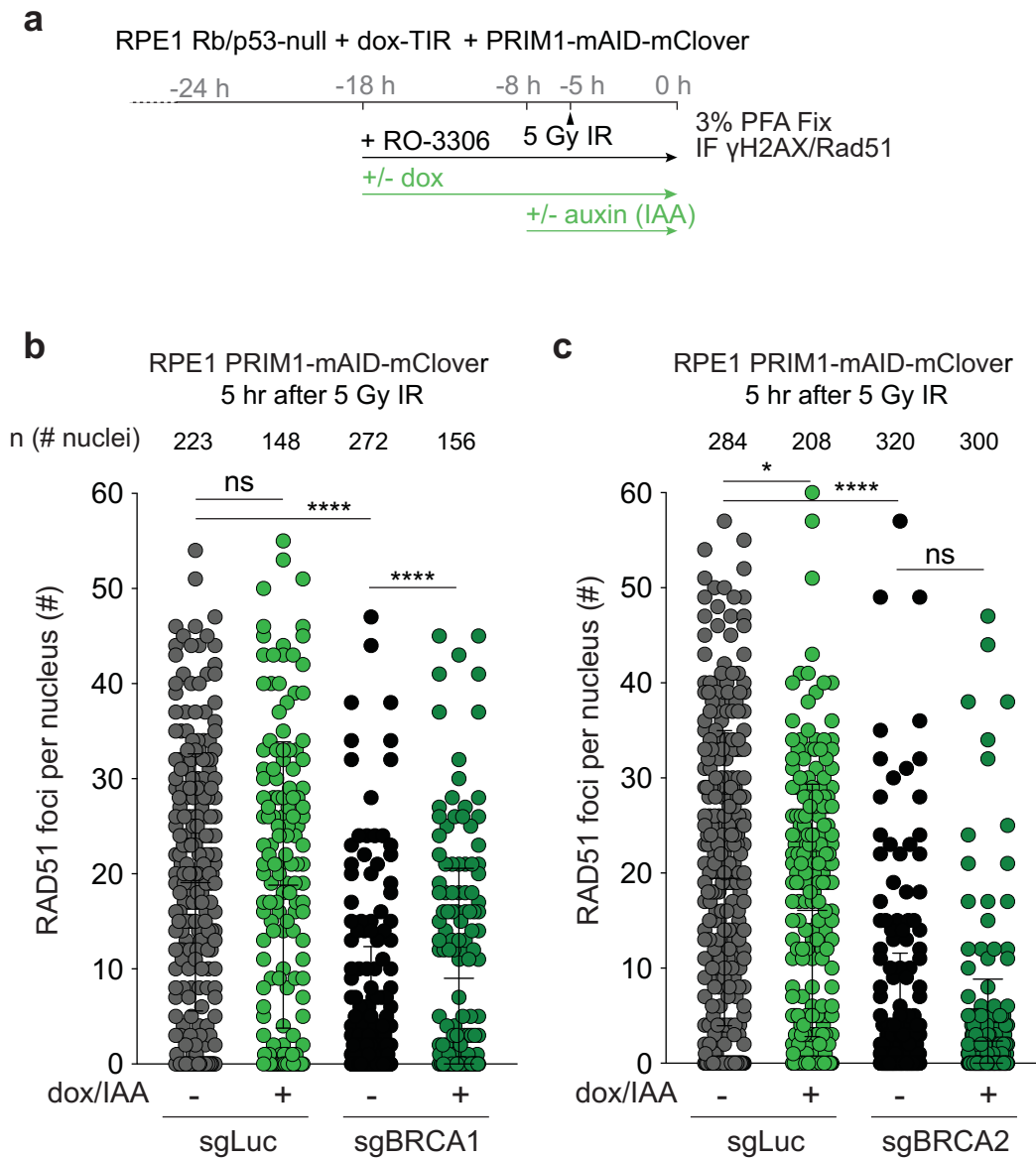
Extended Data Fig. 2 | Primase blocks RAD51 loading in BRCA1-deficient cells (related to Fig. 1). a, Experimental timeline of auxin-induced degradation of PRIM1 in G2-arrested RPE1 cells. 5 hr after 5 Gy IR, cells were harvested for RAD51 IF. **b, c**, Quantification of number of RAD51 foci per nucleus for cells with the indicated treatments. This data is summarized in Fig. 1 **panels e** and **i**. Number of nuclei (n, each represented by a dot) pooled from four independent experiments is indicated. Statistical analyses as in Fig. 1. All means are indicated with center bars and SDs with error bars.
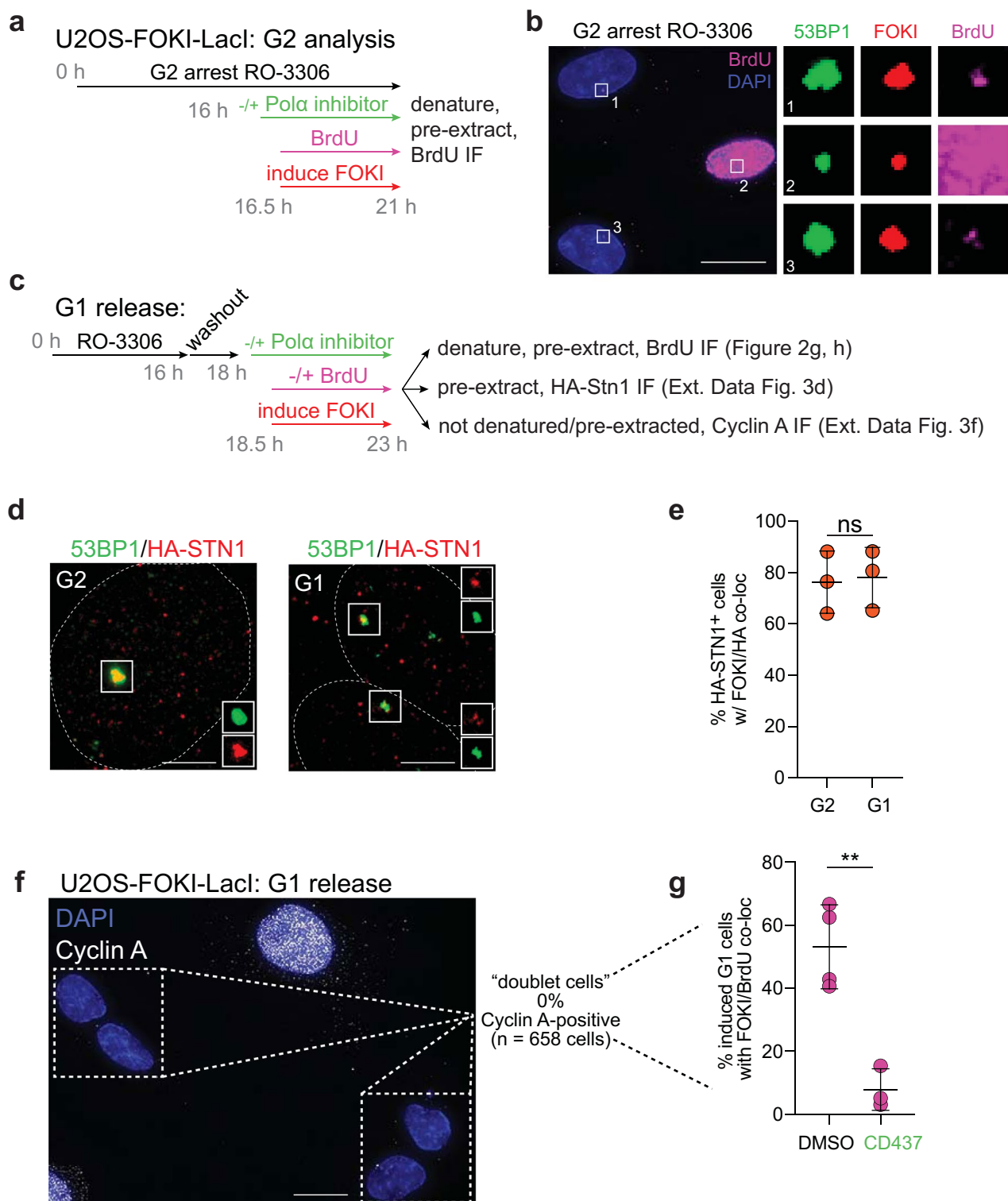
Extended Data Fig. 3 | Experimental setup for detection of fill-in synthesis in U2OS-FOKI cells (related to Fig. 2). a, Experimental timeline for IF to detect BrdU incorporation at DSBs in G2-arrested U2OS cells. **b**, Representative IF images of cells as in **a** visualizing DAPI, 53BP1, mCherry-FOKI, and BrdU. The middle cell displays a global BrdU incorporation pattern, indicative of S phase. Image representative of four independent experiments. Scale bar, 20 μm. **c**, Experimental timeline and IF protocols for U2OS-FOKI-LacI cells released into G1. **d**, Representative IF images of HA-STN1 detected in U2OS-FOKI-LacI cells arrested in G2 with RO-3306 or released into G1 (9 μM RO-3306 overnight followed by washout into fresh media for 2 h before induction of FOKI). Nuclear outlines are demarcated by dashed white lines. Scale bars, 5 μm. **e**, Quantification of HA-STN1 colocalization with FOKI/53BP1 foci in cells as in **d**. n = three independent experiments. **f**, Representative IF for Cyclin A in cells as in **c**. Note the two pairs of small, neighboring, 'doublet' cells, which in all cases were Cyclin A-negative. Such cell pairs are likely to represent the two daughter cells from a recent mitosis. Scale bar, 20 μm. **g**, Quantification of FOKI/BrdU colocalizations in induced, non-S-phase, 'doublet' cells as in **f** after CDKi washout with or without Polα inhibitor. Data from three (CD437) or four (DMSO) independent experiments. Statistical analyses as in Fig. 1. All means are indicated with center bars and SDs with error bars.
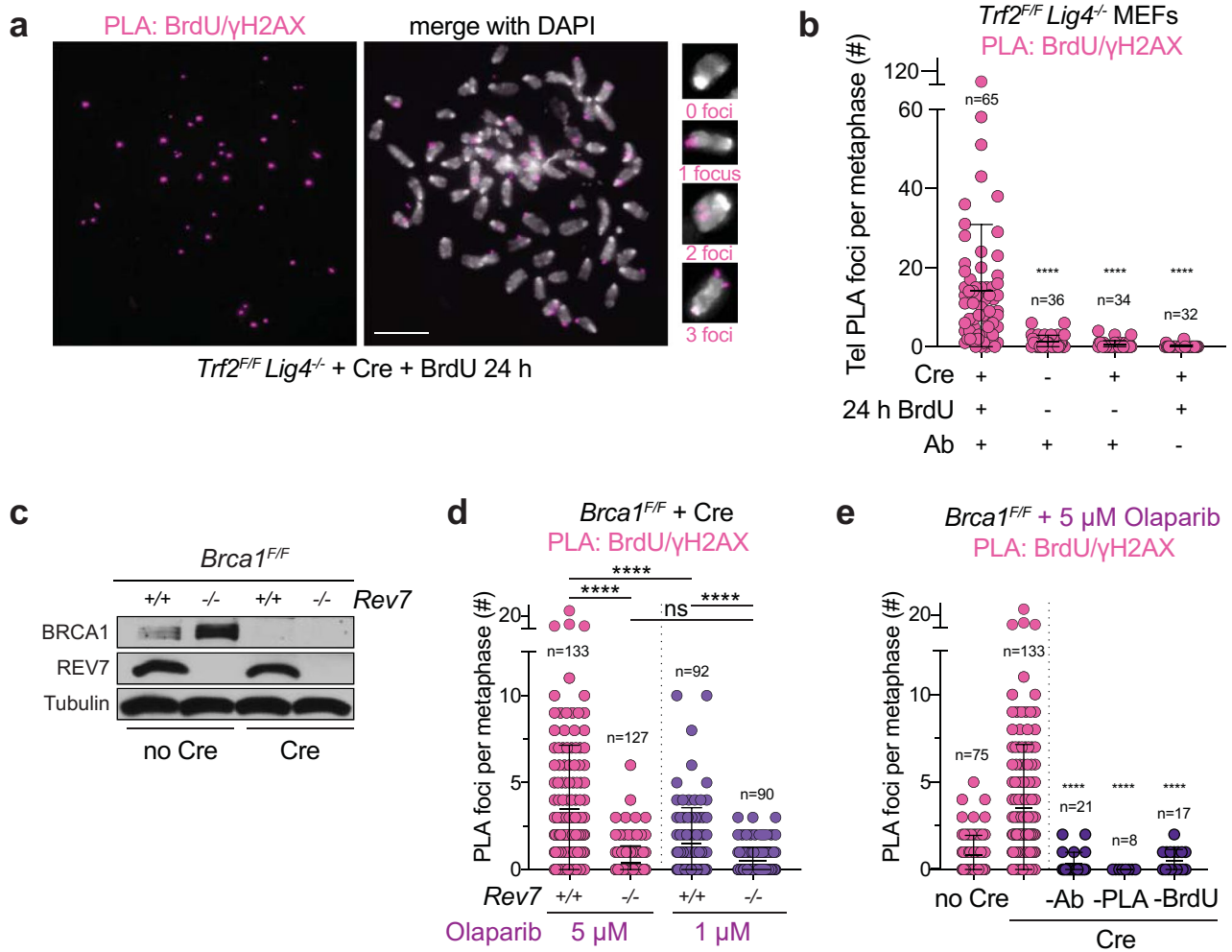
Extended Data Fig. 4 | MetaPLA for detection of fill-in synthesis in BRCA1-deficient cells (related to Fig. 3). a, Representative images from metaPLA of BrdU/γH2AX on metaphase spreads in *Trf2^{F/F} Lig4^{−/−}* MEFs with the indicated treatment that were used to validate the technique. Scale bar, 10 μm. **b**, Quantification of terminal, chromatin-associated BrdU/γH2AX PLA foci for cells as in **a**. **c**, Immunoblot for BRCA1 and REV7 in the indicated cells with or without Cre treatment as in Fig. 3c. Representative of three independent experiments. **d**, Quantification of chromatin-associated BrdU/γH2AX PLA foci on metaphase spreads in *Brca1^{F/F}* MEFs of the indicated genotype, with 5 or 1μM Olaparib. **e**, BrdU/γH2AX PLA controls quantified as in **d**. In b, d, and e, n = the number of metaphases scored in each condition as indicated (n) pooled from three independent experiments. Statistical analyses as in Fig. 1. All means are indicated with center bars and SDs with error bars.
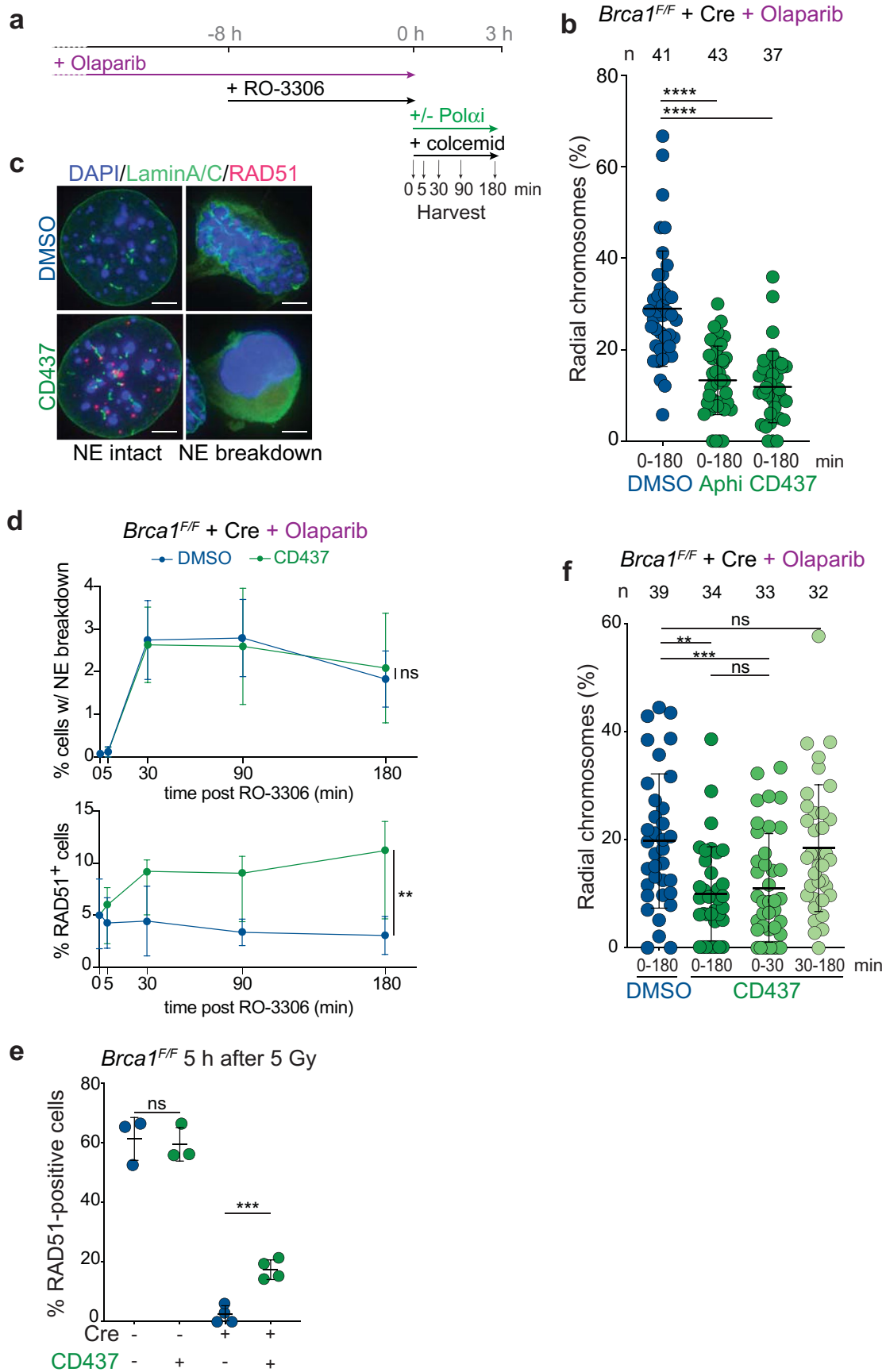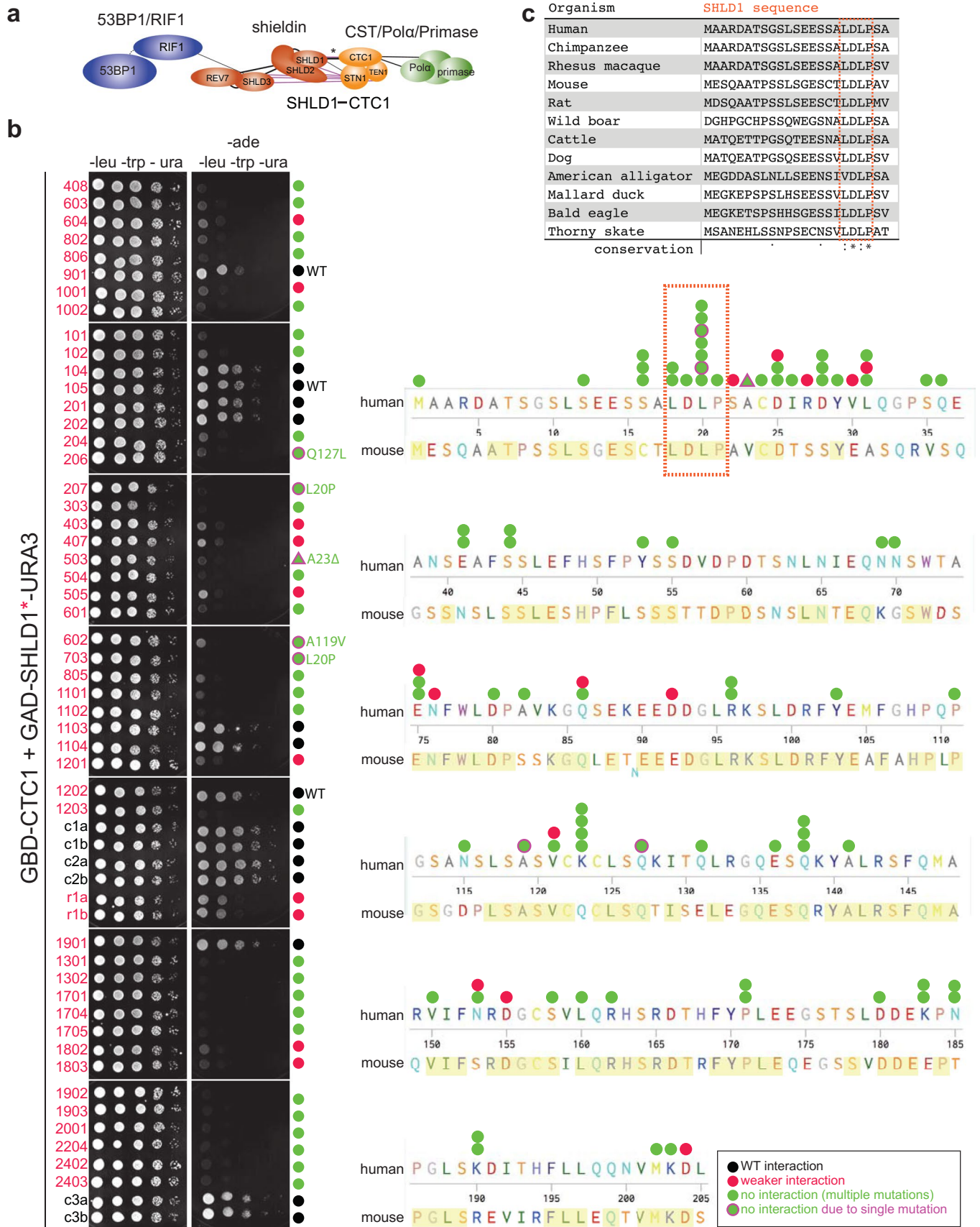
Extended Data Fig. 5 | See next page for caption.

Extended Data Fig. 5 | Fill-in synthesis occurs late in G2 in BRCA1-deficient cells. a, Experimental timeline for Polα inhibition in PARPi-treated, BRCA1-deficient MEFs released from G2 into prolonged (180 min) metaphase arrest. **b**, Quantification of the percent of chromosomes involved in radial structures. Number of metaphases (n, each represented by a dot) pooled from three independent experiments is indicated. **c**, Representative sample images of nuclei with intact or broken-down nuclear envelopes (NE) as assessed by Lamin A/C IF. Scale bars, 5 μm. **d**, Top, analysis of NE breakdown timing after release from G2 in cells as in **a** and **c** assessed at the indicated time points. Bottom, analysis of RAD51 foci formation in the same population of cells. Data from three independent experiments. For NE breakdown, Lamin A/C integrity was visually assessed in at least 800 cells per condition per experiment. For RAD51 foci formation, 50-136 nuclei were analyzed per condition per experiment. **e**, Quantification of RAD51-positive nuclei in *Brca1^{F/F}* MEFs following treatment with Cre and IR. n = three (no Cre) or four (+ Cre) independent experiments. **f**, Quantification of percent of chromosomes involved in radial structures after the indicated treatment. Number of metaphases (n, each represented by a dot) pooled from four independent experiments is indicated. Statistical analyses as in Fig. 1. All means are indicated with center bars and SDs with error bars.
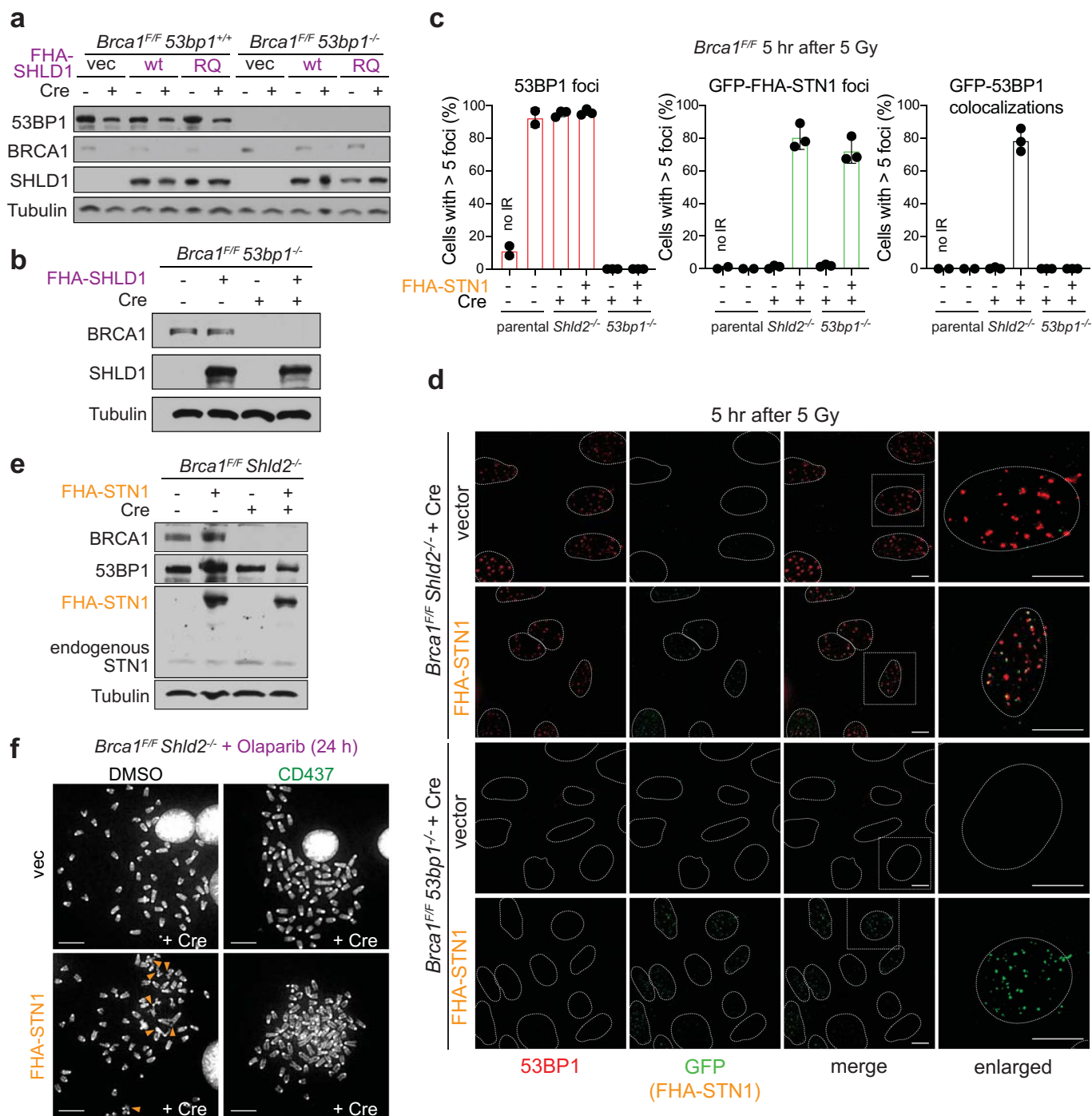
Extended Data Fig. 6 | Bypass of 53BP1/shieldin by artificial tethering of CST (related to Fig. 4). a, Immunoblots for BRCA1, 53BP1, and SHLD1 detecting FHA-SHLD1 in the indicated MEFs expressing FHA-R61Q-SHLD1 (RQ), corresponding to Fig. 4b. **b**, Immunoblots for BRCA1 and SHLD1 detecting FHA-SHLD1 in the indicated MEFs, corresponding to Fig. 4c. **c**, Quantification of 53BP1 and GFP-FHA-STN1 foci at DSBs in the indicated MEFs after IR (n = 3 independent experiments, except for the first two columns, where n = 2 independent experiments. **d**, Representative images of irradiated *Brca1^F/F Shld2^−/−* or *Brca1^F/F 53BP1^−/−* MEFs as in **c**. Nuclear outlines are demarcated by dashed white lines. **e**, Immunoblots for BRCA1, 53BP1, and STN1 detecting endogenous and FHA-STN1 in *Brca1^F/F Shld2^−/−* MEFs as in Fig. 4i. **f**, Representative images of DAPI-stained metaphase spreads from cells as in **e**, corresponding to Fig. 4i. All scale bars, 10 μm. All panels are representative of three independent experiments. All means are indicated with center bars and SDs with error bars.

Extended Data Fig. 7 | See next page for caption.

Extended Data Fig. 7 | Identification of a SHLD1 mutant with impaired CTC1 interaction (related to Fig. 5). a, Schematic of 53BP1 and its downstream effectors. Interactions (lines) based on previous reports[13,18–23]. Black lines, interactions demonstrated by coimmunoprecipitation; purple lines, interactions demonstrated by yeast two-hybrid[19]. Asterisk denotes the SHLD1-CTC1 interaction targeted for disruption in the random mutagenesis screen in **b**. **b**, Mutants identified in a yeast two-hybrid screen for loss of CTC1 binding executed with randomly mutagenized human SHLD1 ORFs. Left, candidate GAD-SHLD1-URA3 variants (red numbers) grow on permissive (-leucine, -tryptophan, -uracil) media. Expression of full-length SHLD1 variants is ensured by growth on media lacking uracil. Several controls are also shown (black numbers, for example, c1a). Variants that fail to grow on selective (-leucine, -tryptophan, -uracil, -adenine) media are indicated with a green circle (or triangle for deletion). Five sequenced variants were attributable to a single mutation (green shape with magenta border). Mutation L20P, deletion of nearby A23, or the mutations A119V or Q127L severely diminished the SHLD1-CTC1 interaction. Right, sequence alignment of human and mouse SHLD1 with conserved residues highlighted in yellow. SHLD1 sequence variants are represented graphically by shapes above the sequence (see legend at bottom). The experiment has been performed once. **c**, Multiple sequence alignment of SHLD1. Conservation symbols are according to Uniprot: asterisks, fully conserved; colon, strong similarity; period, weak similarity. The orange outline highlights the conserved LDLP motif deleted in the SHLD1Δ mutant used in this study.
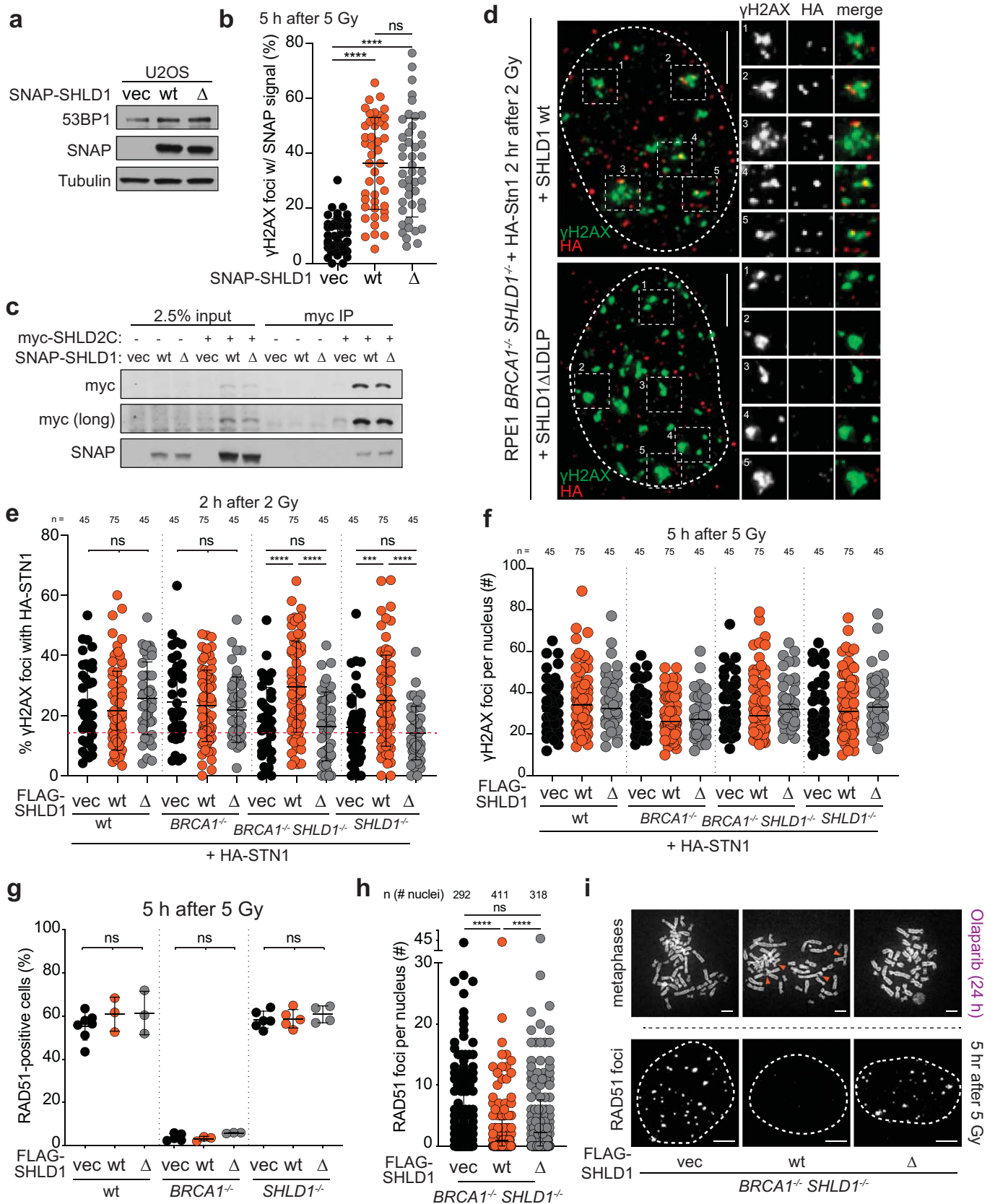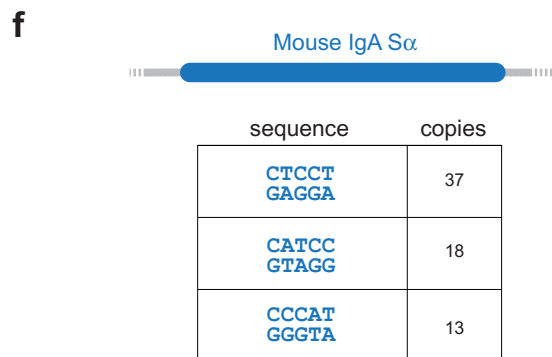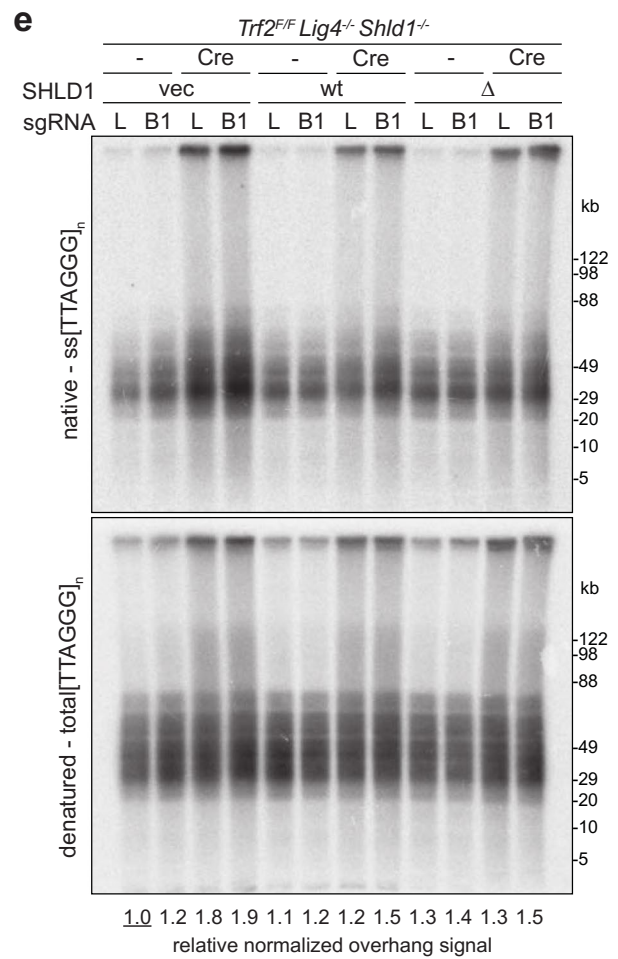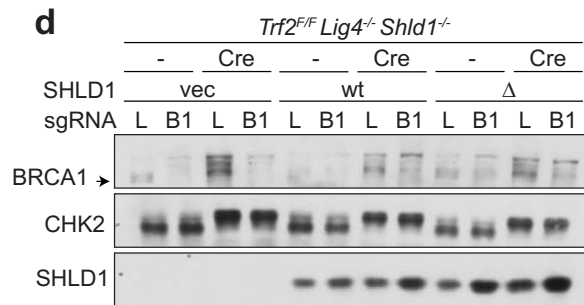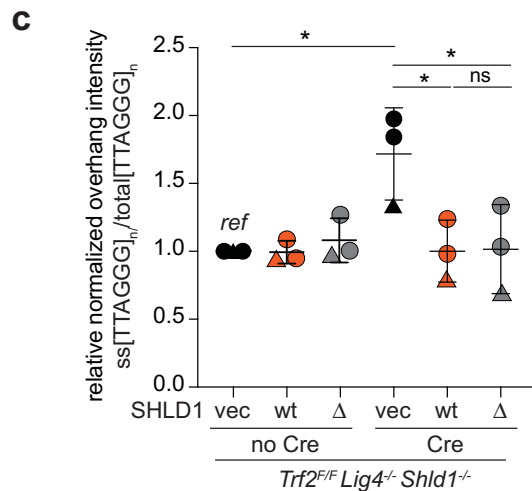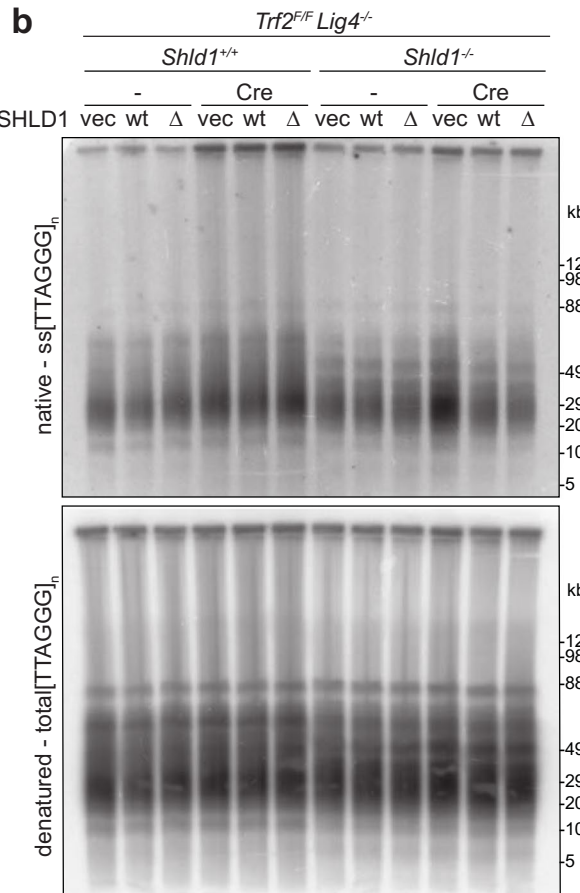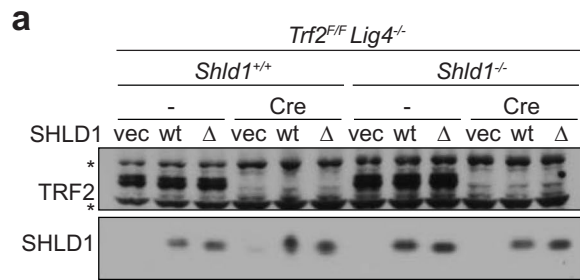
Extended Data Fig. 8 | See next page for caption.

Extended Data Fig. 8 | Characterization of SHLD1Δ (related to Fig. 5). a, Immunoblots showing expression of SNAP-SHLD1 or SNAP-SHLD1ΔLDLP (Δ) in U2OS cells. **b**, Quantification of SNAP-SHLD1 localization to IR-induced γH2AX foci in cells as in **a**. n = 45 nuclei pooled from three independent experiments. **c**, Immunoprecipitation of myc-SHLD2C (aa 421-904) and immunoblot for SNAP-SHLD1 co-expressed in 293 T cells. **d**, Representative IF images showing γH2AX co-localizing with HA-STN1 in irrradiated *BRCA1/SHLD1* DKO cells complemented with wt SHLD1 or SHLD1Δ. Nuclear outlines are demarcated by dashed white lines. Scale bars, 5 μm. Five sample foci are shown for each nucleus. **e**, Quantification of IR-induced γH2AX foci with HA-STN1 signal in the indicated cells. Red dotted line: the average background level across multiple conditions of random overlaps between γH2AX and HA foci (see Materials and Methods). **f**, Quantification of γH2AX foci in the indicated RPE1 cells with HA-STN1 as in **d** and **e**. Center bar indicates median. **g**, Quantification of RAD51 foci as in Fig. 5e in parental (wt), *BRCA1* KO, or *SHLD1* KO RPE1 cells. n = 3-7 independent experiments (as indicated by the number of data points). Ordinary one-way ANOVA was performed with Tukey's correction for multiple comparisons in **g**. **h**, Quantification of the number of RAD51 foci per nucleus for cells as in Fig. 5e with the indicated FLAG-SHLD1 constructs. In **e**, **f**, and **h**, the number of nuclei (n, each represented by a dot) pooled from three independent experiments is indicated. **i**, Representative images of DAPI-stained metaphase spreads (top; orange arrows denote aberrant radial chromosomes) or RAD51 foci (bottom; nuclear outlines demarcated by dashed white lines) in *BRCA1/SHLD1* DKO cells complemented with an empty vector control, wt SHLD1, or SHLD1Δ. Scale bars, 5 μm. a and c are representative of two independent experiments.. Statistical analyses as in Fig. 1. All means are indicated with center bars (unless otherwise noted) and SDs with error bars.
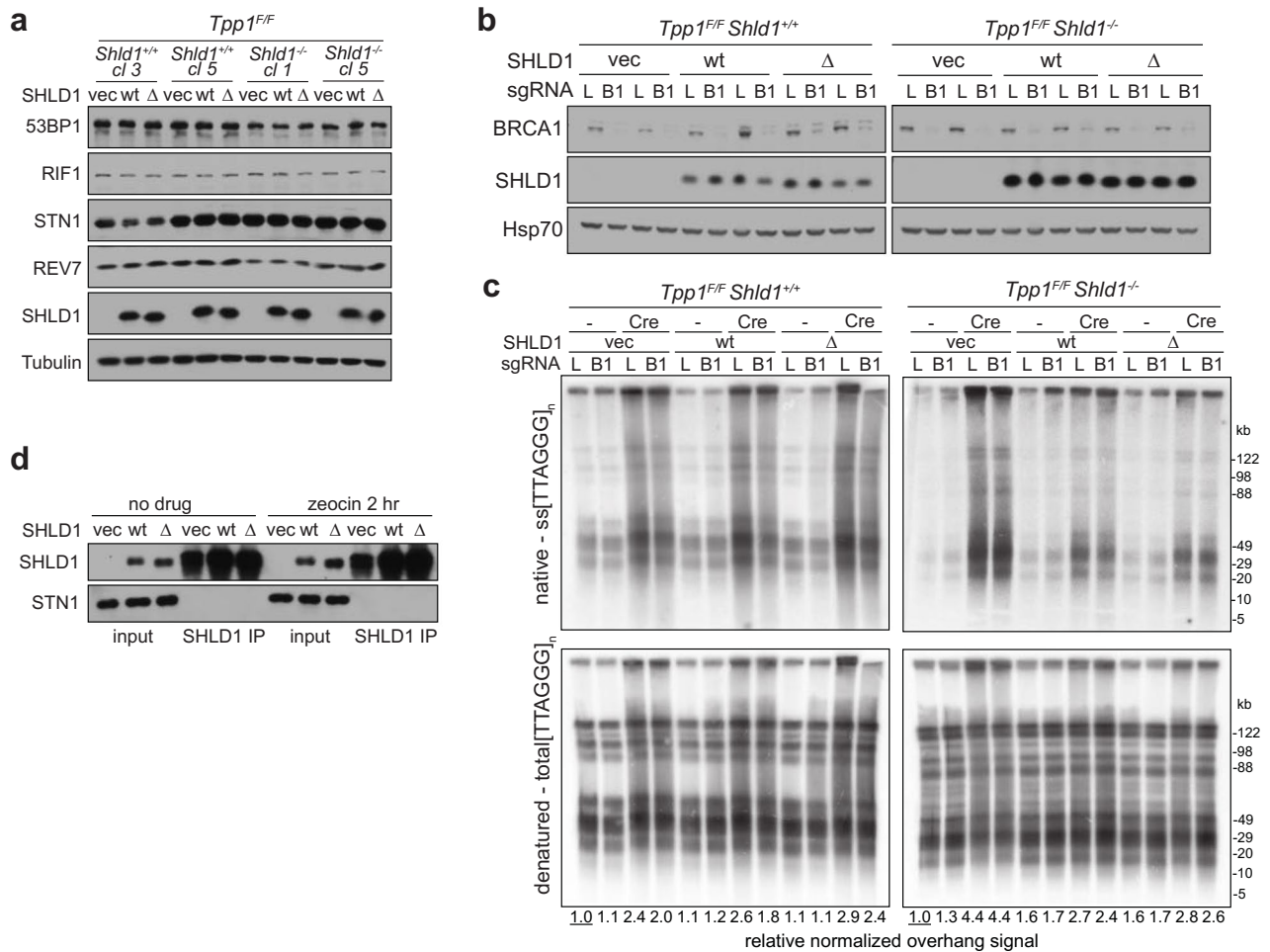
Extended Data Fig. 9 | SHLD1Δ suppresses overhang length at TPP1-deficient telomeres (related to Fig. 6). a, Immunoblot showing expression of 53BP1 pathway components and SHLD1 construct expression in *Tpp1*^F/F^ *Shld1*^+/+^ *or Shld1*^−/−^ clones. **b**, Immunoblot showing bulk CRISPR KO of BRCA1 and SHLD1 construct expression in cells of the indicated genotype with SHLD1 construct expression. **c**, Quantitative analysis of telomeric ss overhang intensity in cells as in **b** using in-gel hybridization to detect the 3' overhang followed by rehybridization to the denatured DNA in the same gel, allowing the ratio of ss to total TTAGGG signal to be determined. **d**, Immunoprecipitation of SHLD1 in *Tpp1*^F/F^ MEFs with the indicated treatments and STN1 immunoblot. Experiments in a-d have been performed once.

a

Trf2^{F/F} Lig4^{-/-}

Shld1^{+/+} | Shld1^{-/-}

- | Cre | - | Cre

SHLD1 vec wt Δ vec wt Δ vec wt Δ vec wt Δ

TRF2

SHLD1

b

Trf2^{F/F} Lig4^{-/-}

Shld1^{+/+} | Shld1^{-/-}

- | Cre | - | Cre

SHLD1 vec wt Δ vec wt Δ vec wt Δ vec wt Δ

native - ss[TTAGGG]_n

kb
-122
-98
-88
-49
-29
-20
-10
-5

denatured - total[TTAGGG]_n

kb
-122
-98
-88
-49
-29
-20
-10
-5

c

SHLD1 vec wt Δ vec wt Δ
no Cre | Cre
Trf2^{F/F} Lig4^{-/-} Shld1^{-/-}

d

Trf2^{F/F} Lig4^{-/-} Shld1^{-/-}

- | Cre | - | Cre | - | Cre

SHLD1 vec | wt | Δ

sgRNA L B1 L B1 L B1 L B1 L B1 L B1

BRCA1 →

CHK2

SHLD1

e

Trf2^{F/F} Lig4^{-/-} Shld1^{-/-}

- | Cre | - | Cre | - | Cre

SHLD1 vec | wt | Δ

sgRNA L B1 L B1 L B1 L B1 L B1 L B1

native - ss[TTAGGG]_n

kb
-122
-98
-88
-49
-29
-20
-10
-5

denatured - total[TTAGGG]_n

kb
-122
-98
-88
-49
-29
-20
-10
-5

1.0 1.2 1.8 1.9 1.1 1.2 1.2 1.5 1.3 1.4 1.3 1.5
relative normalized overhang signal

f

Mouse IgA Sα

sequence	copies
CTCCT GAGGA	37
CATCC GTAGG	18
CCCAT GGGTA	13

Extended Data Fig. 10 | See next page for caption.

Extended Data Fig. 10 | SHLD1Δ suppresses overhang length at TRF2-deficient telomeres (related to Fig. 6). a, Immunoblot showing SHLD1 construct expression and TRF2 deletion by Cre in *Trf2*[F/F] *Lig4*^{−/−} *Shld1*^{+/+} or *Shld1*^{−/−} clones. Asterisks indicate non-specific bands. **b**, Quantitative analysis of telomeric ss overhang intensity in cells as in **a**. **c**, Quantification of overhangs from *Trf2*[F/F] *Lig4*^{−/−} *Shld1*^{−/−} cells (n = 3 independent experiments. **a-c** represent data from three independent experiments using two independent clones (circles and triangle). **d**, Immunoblot showing bulk CRISPR KO of BRCA1 (arrow), phosphorylation of CHK2 after TRF2 deletion, and SHLD1 construct expression. **e**, Telomeric overhang analysis on cells as in **d**. Statistical analysis was performed using two-tailed ratio-paired t-test. *, $p < 0.05$; **, $p < 0.01$; ns, not significant. Experiments in **d, e** have been performed once. **f**, Schematic of mouse IgA Switch region with several five nucleotide repeat sequences and their number of repeats in the region (4.4 kb). All means are indicated with center bars and SDs with error bars.

nature research

Corresponding author(s):   Titia de Lange

Last updated by author(s):   October 19, 2021

Reporting Summary

Nature Research wishes to improve the reproducibility of the work that we publish. This form provides structure for consistency and transparency in reporting. For further information on Nature Research policies, see Authors & Referees and the Editorial Policy Checklist.

Statistics

For all statistical analyses, confirm that the following items are present in the figure legend, table legend, main text, or Methods section.

n/a	Confirmed	
☐	☒	The exact sample size (*n*) for each experimental group/condition, given as a discrete number and unit of measurement
☐	☒	A statement on whether measurements were taken from distinct samples or whether the same sample was measured repeatedly
☐	☒	The statistical test(s) used AND whether they are one- or two-sided *Only common tests should be described solely by name; describe more complex techniques in the Methods section.*
☒	☐	A description of all covariates tested
☐	☒	A description of any assumptions or corrections, such as tests of normality and adjustment for multiple comparisons
☐	☒	A full description of the statistical parameters including central tendency (e.g. means) or other basic estimates (e.g. regression coefficient) AND variation (e.g. standard deviation) or associated estimates of uncertainty (e.g. confidence intervals)
☐	☒	For null hypothesis testing, the test statistic (e.g. *F*, *t*, *r*) with confidence intervals, effect sizes, degrees of freedom and *P* value noted *Give P values as exact values whenever suitable.*
☒	☐	For Bayesian analysis, information on the choice of priors and Markov chain Monte Carlo settings
☒	☐	For hierarchical and complex designs, identification of the appropriate level for tests and full reporting of outcomes
☒	☐	Estimates of effect sizes (e.g. Cohen's *d*, Pearson's *r*), indicating how they were calculated

Our web collection on statistics for biologists contains articles on many of the points above.

Software and code

Policy information about availability of computer code

Data collection	SoftWorx, Typhoon Phosphorimager
Data analysis	FIJI version v 2, Prism v 8, Microsoft Excel v 16.54, FlowJo v 10, Benchling

For manuscripts utilizing custom algorithms or software that are central to the research but not yet described in published literature, software must be made available to editors/reviewers. We strongly encourage code deposition in a community repository (e.g. GitHub). See the Nature Research guidelines for submitting code & software for further information.

Data

Policy information about availability of data

All manuscripts must include a data availability statement. This statement should provide the following information, where applicable:
- Accession codes, unique identifiers, or web links for publicly available datasets
- A list of figures that have associated raw data
- A description of any restrictions on data availability

All data that were generated and/or analyzed in this study are included in the published paper and its Supplementary Information.

Field-specific reporting

Please select the one below that is the best fit for your research. If you are not sure, read the appropriate sections before making your selection.

☒ Life sciences   ☐ Behavioural & social sciences   ☐ Ecological, evolutionary & environmental sciences

For a reference copy of the document with all sections, see nature.com/documents/nr-reporting-summary-flat.pdf

Life sciences study design

All studies must disclose on these points even when the disclosure is negative.

Sample size	No statistical methods were used to predetermine sample size. Sample size was determined based on previous, similar experiments in the lab where the sample size provided statistical power to detect an effect under similar experimental conditions.(Mirman, Z. et al. 53BP1-RIF1-shieldin counteracts DSB resection through CST- and Polα-dependent fill-in. Nature 560, 112-116 (2018); Celli, G. B. & de Lange, T. DNA processing is not required for ATM-mediated telomere damage response after TRF2 deletion. Nat Cell Biol 7, 712-718 (2005))
Data exclusions	No data was excluded from the experiments presented in the study. In the case of experiments which failed for technical reasons (e.g. sample loss; failure of Cre-mediated deletion; cell culture anomalies) all data from the failed experiment was not included in the study.
Replication	Number of independent experiments are reported in figure legends. All immunoblots and sample images are representative of at least three independent experiments (unless otherwise indicated) with similar results.
Randomization	Our in vitro experiments are randomized as much as possible in the sense that culture dishes seeded with identical parental populations of cells were then chosen at random for the various biological perturbations (e.g. treatment with Cre, or not; IR or no radiation; infection with sgRNA vectors).
Blinding	Investigators were not blinded to group allocation during the study, but all samples were processed in parallel and thus treated identically for all experiments. In most experiments, blinding is not applicable because the sample identity is readily apparent to the investigator (e.g., BRCA1-deficient metaphases with radial chromosomes, irradiated cells with IR-induced foci)

Reporting for specific materials, systems and methods

We require information from authors about some types of materials, experimental systems and methods used in many studies. Here, indicate whether each material, system or method listed is relevant to your study. If you are not sure if a list item applies to your research, read the appropriate section before selecting a response.

Materials & experimental systems

n/a	Involved in the study
☐	☒ Antibodies
☐	☒ Eukaryotic cell lines
☒	☐ Palaeontology
☒	☐ Animals and other organisms
☒	☐ Human research participants
☒	☐ Clinical data

Methods

n/a	Involved in the study
☒	☐ ChIP-seq
☐	☒ Flow cytometry
☒	☐ MRI-based neuroimaging

Antibodies

Antibodies used	Immunoblotting was performed as described{Mirman et al., 2018, #105071} with the following antibodies: 53BP1 (175933, Abcam; 1:1000; 100-304, Novus Biological; 1:1000); BRCA1 (MAB22101, R+D systems; 1:500); BRCA2 (OP95, Millipore; 1:500); CHK1 (8408, Santa Cruz; 1:1000); pCHK1 (2341, Cell Signaling Technology; 1:1000); CHK2 (611570, BD; 1:1000); Flag-tag (M2, Sigma; 1:1000); γ-Tubulin (GTU488, Sigma; 1:20,000); GFP (11814460001, Sigma; 1:1000); HA (3724, Cell Signaling Technology; 1:20,000); HSP70 (610608, BD; 1:1000); MAD2L2/REV7 (180579, Abcam; 612266, BD; 1:1000); Myc-tag (9B11, Cell Signaling Technology; 1:1000); OBFC1/STN1 (89250, Abcam; 1:1000; SC-376450, Santa Cruz; 1:1000); PRIM1 (10773-1-AP, Proteintech; 1:1000); RIF1 (#1240, de Lange Lab; 1:1000); SHLD1 (PA5-59280, Thermo-Fisher; 1:1000); SNAP tag (9310, NEB; 1:1000); TRF2 (#1254, de Lange Lab; 1:5,000). Affinity-purified peptide antibodies against mouse SHLD1 and SHLD2 proteins (Chapman Lab, unpublished; 1:1000) were generated by Eurogentec. IF: BrdU (152095, Abcam; 1:500); 53BP1 (612522, BD Biosciences; 1:1000); γH2AX (05636, Millipore; 1:1000); HA (3724, Cell Signaling Technology; 1:5,000); SNAP (9310, NEB; 1:5,000); Cyclin A (611269, BD; 1:1000); Lamin A/C (4200236, Sigma; 1:1000); RAD51 (70-001, Bioacademia; 1:1000). Anti-mouse highly cross-absorbed Alexa fluor plus 488 (1:500) and anti-rabbit highly cross-absorbed Alexa fluor plus 647 (1:500) secondary antibodies were used (Thermo Fisher).
Validation	The following antibodies were validated by comparing wild-type cells to KO cells by western blot and/or immunofluorescence: 53BP1 (Abcam; Novus Biological); BRCA1 (R+D systems); BRCA2 (Millipore); MAD2L2/REV7 (Abcam); OBFC1/STN1 (Abcam; Santa Cruz); PRIM1 (Proteintech); RIF1 (#1240, de Lange Lab); TRF2 (#1254, de Lange Lab). The following antibodies have been used for immunoblot after shelterin deletion: CHK1 (Santa Cruz); pCHK1 (Cell Signaling Technology); CHK2 (BD) (Mirman, Z. et al. 53BP1-RIF1-shieldin counteracts DSB resection through CST- and Polα-dependent fill-in. Nature 560, 112-116 (2018)) The following antibodies were validated based on their use to detect exogenously expressed proteins which were detected at their predicted molecular weight by immunoblotting: Flag-tag (Sigma); GFP (Sigma); HA (Cell Signaling Technology); Myc-tag (Cell Signaling Technology); PRIM1 (Proteintech); SHLD1 (hermo-Fisher); SNAP tag (NEB).

Eukaryotic cell lines

Policy information about cell lines

Cell line source(s)	Brca1F/F Tpp1F/F and Trf2F/FLig4-/- MEFs have been previously described (Mirman, Z. et al. 53BP1-RIF1-shieldin counteracts DSB resection through CST- and Polα-dependent fill-in. Nature 560, 112-116 (2018); Xu, X. et al. Centrosome amplification and a defective G2-M cell cycle checkpoint induce genetic instability in BRCA1 exon 11 isoform-deficient cells. Mol Cell 3, 389-95. (1999); Celli, G. B. & de Lange, T. DNA processing is not required for ATM-mediated telomere damage response after TRF2 deletion. Nat Cell Biol 7, 712-718 (2005)). U2OS cells containing a LacO array and a tamoxifen- and Shield1-ligand-regulated mCherry-FOKI-LacI fusion were used as described (Tang, J. et al. Acetylation limits 53BP1 association with damaged chromatin to promote homologous recombination. Nat Struct Mol Biol 20, 317-325 (2013)). Brca1F/F 53bp1-/- and Brca1F/F Rev7-/- MEFs were previously described (Mirman, Z. et al. 53BP1-RIF1-shieldin counteracts DSB resection through CST- and Polα-dependent fill-in. Nature 560, 112-116 (2018)). Brca1F/F Shld2-/- MEFs were generated by CRISPR/Cas9 targeting exon 4 using the guide 5'-ATCAGTCAGATCCCTGCGTTCGG-(PAM)-3'. Human SHLD1 knockout RPE1 cells were generated by targeting exon 2 of SHLD1 using the sgRNA 5'-TCTCTTATGTCACACGCTGA-(PAM)-3' in BRCA1 KO p53-/- hTERT Cas9 RPE1 cells or an isogenic BRCA1-proficient control(Noordermeer, S. M. et al. The shieldin complex mediates 53BP1-dependent DNA repair. Nature 560, 117-121 (2018)). 293FT and Phoenix Ampho and Eco cells were purchased from ATCC. CH12-F3 cells and CRISPR-Cas9 edited Shld1–/– derivatives were previously described (Ghezraoui et al., Nature (2018)).
Authentication	BRCA1F/F and TRF2F/FLig4-/- MEF cell lines were confirmed by western blot. Tpp1F/F has been validated by IF, WB, and telomeric overhang blot. For all CRISPR-generated clones, bi-allelic gene disruption was verified by Sanger sequencing of Topo-cloned PCR products of the relevant locus (sequences available on request) and clones were confirmed by western blot if possible. The human cell lines were verified based on the appropriate cell biological read-outs (i.e., induction of FOKI cut) and/or by western blot.
Mycoplasma contamination	No mycoplasma contaminations were found in the course of these experiments
Commonly misidentified lines (See ICLAC register)	No commonly misidentified cell lines were used in this study.

Flow Cytometry

Plots

Confirm that:

☒ The axis labels state the marker and fluorochrome used (e.g. CD4-FITC).

☒ The axis scales are clearly visible. Include numbers along axes only for bottom left plot of group (a 'group' is an analysis of identical markers).

☒ All plots are contour plots with outliers or pseudocolor plots.

☒ A numerical value for number of cells or percentage (with statistics) is provided.

Methodology

Sample preparation	Stimulated CH12F3 cell lines were washed with PBS, 2% BSA and 0.025% sodium azide (FACS buffer) and then stained for cell surface markers as per the methods section on ice for 20 min in FACS buffer. Cells were washed and resuspended in FACS buffer before acquisition.
Instrument	Samples were acquired on an Attune NxT (Life Technologies)
Software	Samples were analysed using FlowJo v10 (Tree Star)
Cell population abundance	N/A. No sorting was performed, so determining cell population in post-sort fractions is not applicable. Sufficient cells were obtained under all biological conditions for flow cytometric monitoring of class switch recombination as previously described (Ghezraoui et al. Nature, 2018)
Gating strategy	Stimulated CH12F3 analysis: cells that successfully underwent class switch recombination were identified as singlet IgA+.

☒ Tick this box to confirm that a figure exemplifying the gating strategy is provided in the Supplementary Information.